arXiv:1507.02784v1 [physics.flu-dyn] 10 Jul 2015

Branch cuts of Stokes wave on deep water. Part I: Numerical solution and Padé approximation

Sergey A. Dyachenko[1,2], Pavel M. Lushnikov[3,4]†, and Alexander O. Korotkevich[3,4]

[1]Department of Mathematics, University of Illinois at Urbana-Champaign, 1409 W. Green Street, Urbana, IL 61801, USA

[2]Department of Mathematics, University of Arizona, 617 N. Santa Rita Ave., P.O. Box 210089, Tucson, AZ 85721, USA

[3]Department of Mathematics and Statistics, University of New Mexico, Albuquerque, MSC01 1115, NM, 87131, USA

[4]Landau Institute for Theoretical Physics, 2 Kosygin Str., Moscow, 119334, Russia

(Received 29 January 2022)

Complex analytical structure of Stokes wave for two-dimensional potential flow of the ideal incompressible fluid with free surface and infinite depth is analyzed. Stokes wave is the fully nonlinear periodic gravity wave propagating with the constant velocity. Simulations with the quadruple (32 digits) and variable precisions (more than 200 digits) are performed to find Stokes wave with high accuracy and study the Stokes wave approaching its limiting form with $2\pi/3$ radians angle on the crest. A conformal map is used which maps a free fluid surface of Stokes wave into the real line with fluid domain mapped into the lower complex half-plane. The Stokes wave is fully characterized by the complex singularities in the upper complex half-plane. These singularities are addressed by rational (Padé) interpolation of Stokes wave in the complex plane. Convergence of Padé approximation to the density of complex poles with the increase of the numerical precision and subsequent increase of the number of approximating poles reveals that the only singularities of Stokes wave are branch points connected by branch cuts. The converging densities are the jumps across the branch cuts. There is one branch cut per horizontal spatial period λ of Stokes wave. Each branch cut extends strictly vertically above the corresponding crest of Stokes wave up to complex infinity. The lower end of branch cut is the square-root branch point located at the distance v_c from the real line corresponding to the fluid surface in conformal variables. The increase of the scaled wave height H/λ from the linear limit $H/\lambda = 0$ to the critical value H_{max}/λ marks the transition from the limit of almost linear wave to a strongly nonlinear limiting Stokes wave (also called by the Stokes wave of the greatest height). Here H is the wave height from the crest to the trough in physical variables. The limiting Stokes wave emerges as the singularity reaches the fluid surface. Tables of Padé approximation for Stokes waves of different heights are provided. These tables allow to recover the Stokes wave with the relative accuracy of at least 10^{-26}. The tables use from several poles for near-linear Stokes wave up to about hundred poles to highly nonlinear Stokes wave with $v_c/\lambda \sim 10^{-6}$.

Key words:

† Email address for correspondence: plushnik@math.unm.edu

1. Introduction

Theory of spatially periodic progressive (propagating with constant velocity without change of the shape and amplitude) waves in two-dimensional (2D) potential flow of an ideal incompressible fluid with free surface in gravitational field was founded in pioneering works by Stokes (1847, 1880*a*) and developed further by Michell (1893), Nekrasov (1921, 1951), and many others (see e.g. a book by Sretenskii (1976) for review of older works as well as Baker & Xie (2011); Cowley *et al.* (1999); Grant (1973); Longuet-Higgins (2008); Longuet-Higgins & Fox (1977, 1978); Schwartz (1974); Tanveer (1991); Williams (1981, 1985) and references there in for more recent progress). There are two major approaches to analyze the Stokes wave, both originally developed by Stokes. The first approach is the perturbation expansion in amplitude of Stokes wave called by the Stokes expansion. That approach is very effective for small amplitudes but converges very slowly (or does not converge at all, depending on the formulation according to Drennan *et al.* (1992)) as the wave approaches to the maximum height $H = H_{max}$ (also called by the Stokes wave of the greatest height or the limiting Stokes wave). Here the height H is defined at the vertical distance from the crest to the trough of Stokes wave over a spatial period λ. The second approach is to consider the limiting Stokes wave, which is the progressive wave with the highest nonlinearity. Using conformal mappings Stokes found that the limiting Stokes wave has the sharp angle of $2\pi/3$ radians on the crest (Stokes 1880*b*), i.e. the surface is non-smooth (has a jump of slope) at that spatial point. That corner singularity explains a slow convergence of Stokes expansion as $H \to H_{max}$. The global existence of the limiting Stokes wave was proven by Toland (1978) however lacking a proof of a Stokes conjecture that the the jump of the slope at the crest is exactly $2\pi/3$ radians. The Stokes conjecture was later independently proven by Plotnikov (1982) and Amick *et al.* (1982).

It was Stokes (1880*b*) who first proposed to use conformal mapping in order to address finite amplitude progressive waves. In this paper we consider a particular case of potential flow of the ideal fluid of infinite depth although more general case of fluid of arbitrary depth can be studied in a similar way. Assume that free surface is located at $y = \eta(x,t)$, where x is the horizontal coordinate, y is the vertical coordinate, t is the time and $\eta(x,t)$ is the surface elevation with respect to the zero mean level of fluid, i.e. $\int_{-\infty}^{\infty} \eta(x,t)\mathrm{d}x = 0$. We consider the conformal map between the domain $-\infty < y \leqslant \eta(x,t),\ -\infty < x < \infty$ of the complex plane $z \equiv x + \mathrm{i}y$ filled by the infinite depth fluid and a lower complex half-plane (from now on denoted by $\mathbb{C}^-$) of a variable $w \equiv u + \mathrm{i}v$ (see Fig. 1). The real line $v = 0$ is mapped into the free surface by $z(w)$ being the analytic function in the lower half-plane of w as well as the complex fluid velocity potential $\Pi(w)$ is also analytic in $\mathbb{C}^-$. Both $z(w)$ and $\Pi(w)$ have singularities in upper half-plane (here and further denoted by $\mathbb{C}^+$).

The knowledge of singularities in $\mathbb{C}^+$ would result in the efficient description of the solution in the physical variables. Examples of such type of solutions in hydrodynamic-type systems are numerous including e.g. the dynamics of free surface of ideal fluid with infinite depth (Kuznetsov *et al.* 1993, 1994; Tanveer 1993) and finite depth (Dyachenko *et al.* 1996*b*), dynamics of interface between two ideal fluids (Kuznetsov *et al.* 1993), ideal fluid pushed through viscous fluid in a narrow gap between two parallel plates (Hele-Shaw flow) (Mineev-Weinstein *et al.* 2000), the dynamics of the interface between ideal fluid and light viscous fluid (Lushnikov 2004) and bubble pinch-off (Turitsyn *et al.* 2009). In these systems the dynamics is determined by poles/branch cuts in the complex plane. Related systems correspond to the spontaneous appearance of curvature singularities on vortex sheets as obtained by Moore (1979). Nie & Baker (1998) established that Moore's

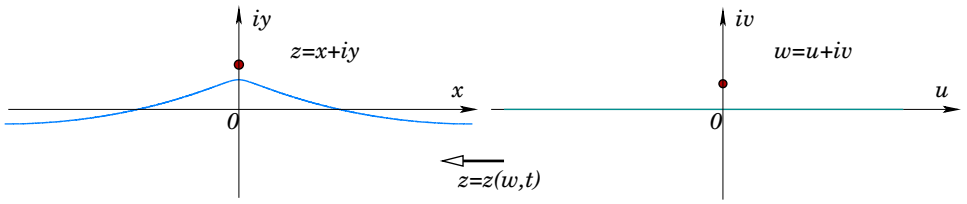


FIGURE 1. Schematic of a conformal map between the domain below the solid curve (left panel) in $z = x + \mathrm{i}y$ complex plane and the lower complex half-plane in $w = u + \mathrm{i}v$ (right panel). Fluid occupies the domain below the solid curve in physical plane $z = x + \mathrm{i}y$. The solid curve of left panel (corresponds to a free surface of the fluid) is mapped into the real line (another solid line) in right panel. One spatial period of Stokes wave is shown by solid lines in both panels in the reference frame moving with the velocity c. The dark circles mark the positions of the singularity closest to the fluid surface in both panels.

singularities are present in axisymmetric vortex sheets. Inogamov & Oparin (2003) considered cone-shaped nose of $2\pi/3$ degrees in axisymmetric flow. Ishihara & Kaneda (1994) and Hou & Hu (2003) extended Moore's singularities to three-dimensional (3D) vortex sheets. Opposite limit is the global existence of water waves for small enough data shown both for 2D (Wu 2009) and 3D (Wu 2011) flows.

In this paper we determine that for Stokes wave the lowest singularities in $\mathbb{C}^+$ of both $z(w)$ and $\Pi(w)$ are the square-root branch points located periodically at $w = n\lambda + \mathrm{i}v_c - ct,\ n = 0, \pm1, \pm2, ...$ (we choose the crests of Stokes wave to be located at $w = n\lambda - ct$) and we determine v_c numerically as a function of H/λ. Here c is the velocity of propagation of Stokes wave which depends on H. In the previous work Dyachenko *et al.* (2013) we found that as $H \to H_{max}$, the branch point approaches real axis with the scaling law

$$v_c \propto (H_{max} - H)^{\delta}, \tag{1.1}$$

where $\delta = 1.48 \pm 0.03$. We also provided an accurate estimation of maximum amplitude of the Stokes wave H_{max}. Adiabatically slow approach of Stokes wave to its limiting form during wave dynamics is one of the possible routes to wave breaking and whitecapping, which are responsible for significant part of energy dissipation for gravity waves (Zakharov *et al.* 2009, 2007). Formation of a close to limiting Stokes wave is also considered to be a probable final stage of evolution of a freak (or rogue) waves in the ocean resulting in formation of approximate limiting Stokes wave for a limited period of time with following wave breaking and disintegration of the wave or whitecapping and attenuation of the freak wave into wave of regular amplitude (Rainey & Longuet-Higgins 2006; Zakharov *et al.* 2006).

The paper is organized as follows. In Section 2 we introduce the basic equations of 2D hydrodynamics in conformal conformal variables and reduce these equations to the equation for Stokes wave. In Section 3 numerical approaches to simulation of Stokes wave are given together with the results of simulations. Also numerical procedures to recover the location and type of the branch point are discussed. Section 4 introduces a new variable ζ defining a second conformal transformation which maps one spatial period of Stokes wave into the entire real line. Then the Padé approximation of Stokes wave is found in complex ζ plane. The efficient Alpert-Greengard-Hagstrom (AGH) algorithm (Alpert *et al.* 2000; Lau 2004) is used to obtain the Padé approximation. That algorithm allows to avoid the appearance of artificial zeros and poles of Padé approximation and achieves a spectral accuracy. The convergence of the Padé approximation to the branch cut singularity is established which allows to recover the jump at branch cut. Section 5

relates jump at the branch cut in ζ variable to the sum of periodically located branch cuts in w complex plane. It is shown how to use the series expansion of the jump along branch cuts near branch points to recover the square-root singularity at the branch point. It is demonstrated that there are no more singularities in the finite complex plane beyond one branch point $w = \mathrm{i}v_c$ per period. In Section 6 the main results of the paper are discussed. Appendix A provides a derivation of basic hydrodynamic equations in conformal variables. Appendix B gives a short description of AGH algorithm adapted for Stokes wave. Appendix C describes a notation used for the tables of Padé approximants for Stokes wave and gives samples of such tables. A full set of tables is provided in the electronic attachment. These tables reproduce the Stokes wave with the relative accuracy of at least 10^{-26}.

2. Basic equations

In physical coordinates (x, y) a velocity $\mathbf{v}$ of $2D$ potential flow of inviscid incompressible fluid is determined by a velocity potential $\Phi(x, y, t)$ as $\mathbf{v} = \nabla\Phi$. The incompressibility condition $\nabla \cdot \mathbf{v} = 0$ results in the Laplace equation

$$\nabla^2\Phi = 0 \tag{2.1}$$

inside fluid $-\infty < y < \eta(x, t)$. To obtain the closed set of equations we add the decaying boundary condition at large depth $\Phi(x, y, t)|_{y\to-\infty} = 0$, the kinematic boundary condition

$$\frac{\partial\eta}{\partial t} = \left(-\frac{\partial\eta}{\partial x}\frac{\partial\Phi}{\partial x} + \frac{\partial\Phi}{\partial y}\right)\Big|_{y=\eta(x,t)} \tag{2.2}$$

and the dynamic boundary condition

$$\left(\frac{\partial\Phi}{\partial t} + \frac{1}{2}\left(\nabla\Phi\right)^2\right)\Big|_{y=\eta(x,t)} + g\eta = 0 \tag{2.3}$$

at the free surface

$$y = \eta(x, t). \tag{2.4}$$

We define the boundary value of the velocity potential as

$$\Phi(x, y, t)|_{y=\eta(x,t)} \equiv \psi(x, t), \tag{2.5}$$

Consider a time-dependent conformal transformation

$$z = z(w, t), \quad w = u + iv \tag{2.6}$$

which maps a half-strip $-\frac{\lambda}{2} \leqslant u < \frac{\lambda}{2},\ -\infty < v \leqslant 0$ of complex plane w into a region $-\frac{\lambda}{2} \leqslant x < \frac{\lambda}{2},\ -\infty < y \leqslant \eta(x, t)$ of complex physical plane $z = x + \mathrm{i}y$ at each time t such that the line $-\frac{\lambda}{2} \leqslant u < \frac{\lambda}{2},\ v = 0$ is mapped into a line of free surface $x + \mathrm{i}\eta(x, t)$ with $-\frac{\lambda}{2} \leqslant x < \frac{\lambda}{2}$ and

$$x\left(-\frac{\lambda}{2}\right) = -\frac{\lambda}{2}, \quad x\left(\frac{\lambda}{2}\right) = \frac{\lambda}{2}. \tag{2.7}$$

Also $w = -\mathrm{i}\infty$ maps into $z = -\mathrm{i}\infty$. Here the flow is assumed to be periodic in the horizontal direction with the period λ both in w and z variables. Conditions (2.7) suggest to separate $z(w, t)$ into a periodic part $\tilde{z}(w, t)$ and a non-periodic part w as follows

$$z(w, t) = w + \tilde{z}(w, t), \text{ or } x(w, t) = u + \tilde{x}(w, t), \quad \tilde{y}(w, t) = v + y(w, t), \tag{2.8}$$

where

$$\tilde{z}(w+\lambda) = \tilde{z}(w), \quad \tilde{x}\left(\pm\frac{\lambda}{2}\right) = 0. \tag{2.9}$$

Equations (2.8) and (2.9) extend conformal transformation (2.6) into $\mathbb{C}^-$. Also $x(u,t)$ and $y(u,t)$ form a parametric representation (over the parameter u) of the free surface elevation (2.4).

The idea of using time-dependent conformal transformation for unsteady fluid flow was exploited by several authors including Ovsyannikov (1973), Meison *et al.* (1981), Tanveer (1991, 1993), and Dyachenko *et al.* (1996*a*); Zakharov *et al.* (2002*b*). We follow Dyachenko *et al.* (1996*a*) to recast the system (2.1)-(2.3) into the equivalent form for $x(u,t)$, $y(u,t)$ and $\psi(u,t)$ at the real line $w = u$ of the complex plane w using the conformal transformation (2.6) (see Appendix A for more details). A kinematic boundary condition (2.2) is reduced to

$$y_t x_u - x_t y_u + \hat{H}\psi_u = 0 \tag{2.10}$$

and the dynamic boundary condition (2.3) is given by

$$\psi_t y_u - \psi_u y_t + g y y_u = -\hat{H}\left(\psi_t x_u - \psi_u x_t + g y x_u\right), \tag{2.11}$$

where

$$\hat{H}f(u) = \frac{1}{\pi}\text{p.v.}\int_{-\infty}^{+\infty}\frac{f(u')}{u'-u}\mathrm{d}u' \tag{2.12}$$

is the Hilbert transform with p.v. meaning a Cauchy principal value of integral. Periodicity of $f(u)$ allows to reduce the integration in the Hilbert transform as follows

$$\hat{H}f(u) = \frac{1}{\pi}\sum_{n=\infty}^{\infty}\text{p.v.}\int_{-\lambda/2}^{\lambda/2}\frac{f(u')}{u'-u+n\lambda}\mathrm{d}u' = \frac{1}{\lambda}\text{p.v.}\int_{-\lambda/2}^{\lambda/2}\frac{f(u')}{\tan\left(\pi\frac{u'-u}{\lambda}\right)}\mathrm{d}u'. \tag{2.13}$$

The equivalence of equations (2.10) and (2.11) to equations (2.1)-(2.3) uses the analyticity of $z(w)$ and $\Pi(w)$ in $\mathbb{C}^-$, where

$$\Pi = \Phi + \mathrm{i}\Theta \tag{2.14}$$

is the complex velocity potential. Here Θ is the stream function defined by $\Theta_x = -\Phi_y$ and $\Theta_y = \Phi_x$ to satisfy Cauchy-Riemann conditions for analyticity of $\Pi(z,t)$ in z plane. The conformal transformation (2.6) ensures that

$$\Theta_u = -\Phi_v, \quad \Theta_v = \Phi_u \tag{2.15}$$

in w plane. The periodicity of the flow implies the condition

$$\Pi(w+\lambda,t) = \Pi(w,t) \tag{2.16}$$

together with equation (2.9). We also assumed in equations (2.10) and (2.11) that

$$\int_{-\lambda/2}^{\lambda/2}\eta(x,t)\mathrm{d}x = \int_{-\lambda/2}^{\lambda/2}y(u,t)x_u(u,t)\mathrm{d}u = 0, \tag{2.17}$$

meaning that the elevation of free surface of unperturbed fluid is set to zero. The equation (2.17) is valid at all times and reflects a conservation of the total mass of fluid.

Both equations (2.10) and (2.11) are defined on the real line $w = u$. The Hilbert operator $\hat{H}$ transforms into the multiplication operator

$$(\hat{H}f)_k = \mathrm{i}\,\mathrm{sign}\,(k)\,f_k, \tag{2.18}$$

for the Fourier coefficients (harmonics) f_k,

$$f_k = \frac{1}{\lambda}\int\limits_{-\lambda/2}^{\lambda/2} f(u)\exp\left(-\mathrm{i}ku\frac{2\pi}{\lambda}\right)\mathrm{d}u, \tag{2.19}$$

of the periodic function $f(u) = f(u+\lambda)$ represented through the Fourier series

$$f(u) = \sum_{k=-\infty}^{\infty} f_k \exp\left(\mathrm{i}ku\frac{2\pi}{\lambda}\right). \tag{2.20}$$

Here $\mathrm{sign}(k) = -1, 0, 1$ for $k<0,\ k=0$ and $k>0$, respectively.

The Fourier series (2.20) allows to rewrite $f(u) = f(w)|_{v=0}$ as follows

$$f(u) = f^+(u) + f^-(u) + f_0, \tag{2.21}$$

where

$$f^+(w) = \sum_{k=1}^{\infty} f_k \exp\left(\mathrm{i}kw\frac{2\pi}{\lambda}\right) \tag{2.22}$$

is the analytical function in $\mathbb{C}^+$,

$$f^-(w) = \sum_{k=-\infty}^{-1} f_k \exp\left(\mathrm{i}kw\frac{2\pi}{\lambda}\right) \tag{2.23}$$

is the analytical function in $\mathbb{C}^-$ and $f_0 = const$ is the zero harmonic of Fourier series (2.20). In other words, equation (2.21) decompose $f(u)$ into the sum of functions $f^+(u)$ and $f^-(u)$ which are analytically continued from the real line $w=u$ into $\mathbb{C}^+$ and $\mathbb{C}^-$, respectively. Equations (2.18), (2.21), (2.22) and (2.23) imply that

$$\hat{H}f(u) = \mathrm{i}\left[f^+(u) - f^-(u)\right]. \tag{2.24}$$

If function $f(w)$ is analytic in $\mathbb{C}^-$ then $\bar{f}(\bar{w})$ is analytic in $\mathbb{C}^+$ as follows from equations (2.21)-(2.23), where bar mean complex conjugation, $\bar{w} = u - \mathrm{i}v$. Then the function $\bar{f}(u)$, $u\in\mathbb{R}$ has analytic continuation into $\mathbb{C}^+$ because at the real line $w=\bar{w}$. Using equations (2.5) and (2.14) we obtain that $\psi(u,t) = \frac{1}{2}[\Pi(u,t) + \bar{\Pi}(u,t)]$. It means that after solving equations (2.10) and (2.11) one can recover the complex potential Π from the analytical continuation of

$$\Pi(u,t) = 2\hat{P}\psi(u,t) \tag{2.25}$$

into $\mathbb{C}^-$. Here

$$\hat{P} = \frac{1}{2}(1 + \mathrm{i}\hat{H}) \tag{2.26}$$

is the projector operator, $\hat{P}f = f^- + \frac{f_0}{2}$, into a function which has analytical continuation from the real line $w=u$ into $\mathbb{C}^-$, as follows from equation (2.24). Note that without loss of generality we assumed the vanishing zero Fourier harmonic, $\Pi_0 = 0$, for $\Pi(u,t)$.

Also

$$\hat{H}^2 f = -f \tag{2.27}$$

for the function $f(u)$ defined by (2.21) provided the additional restriction that $f_0 = 0$ holds. In other words, the Hilbert transformation is invertible on the class of functions represented by their Fourier series provided zeroth Fourier harmonic f_0 vanishes. If $f_0 \neq 0$ then the identity (2.27) is replaced by

$$\hat{H}^2 f = -(f - f_0). \tag{2.28}$$

The analyticity of $z(w)$ in $\mathbb{C}^-$ implies, together with $\tilde{x} = \frac{1}{2}(\tilde{z} + \bar{\tilde{z}})$, $\tilde{y} = \frac{1}{2i}(\tilde{z} - \bar{\tilde{z}})$ and equations (2.24),(2.28), that at the real line $w = u$ the following relations hold

$$y - \tilde{y}_0 = \hat{H}\tilde{x} \quad \text{and} \quad \tilde{x} - \tilde{x}_0 = -\hat{H}y. \tag{2.29}$$

Here $\tilde{x}_0$ and $\tilde{y}_0$ are zero Fourier harmonics of $\tilde{x}(u,t)$ and $y(u,t)$, respectively. Note that the addition of zero harmonics $\tilde{x}_0$ and $\tilde{y}_0$ into equation (2.29) is the modification compare with Refs. Dyachenko *et al.* (1996*a*); Zakharov *et al.* (2002*a*). These Refs. were focused on the decaying boundary conditions $\eta(x,t) \to 0$ and $\psi(x,t) \to 0$ for $|x| \to \infty$ which imply, together with the condition (2.17) in the limit $\lambda \to \infty$, that $\tilde{x}_0 = \tilde{y}_0 = 0$. However, generally $\tilde{x}_0$ and $\tilde{y}_0$ might be nonzero for the periodic solutions with a finite λ considered in this paper.

Equations (2.29) imply that it is enough to find either $y(u,t)$ or $x(u,t)$ then the second of them is recovered by these explicit expressions. Taking derivative of equations (2.29) with respect to u results in the similar relations

$$y_u = \hat{H}\tilde{x}_u \quad \text{and} \quad \tilde{x}_u = -\hat{H}y_u, \tag{2.30}$$

2.1. *Progressive waves*

Stokes wave corresponds to a solution of the system (2.10) and (2.11) in the traveling wave form

$$\psi(u,t) = \psi(u - ct), \ \tilde{z}(u,t) = \tilde{z}(u - ct), \tag{2.31}$$

where both ψ and $\tilde{z}$ are the periodic functions of $u - ct$. Here c is the phase velocity of Stokes wave. We transform into the moving frame of reference, $u - ct \to u$, and assume that the crest of the Stokes wave is located at $u = 0$ as in Fig. 1 and λ is the spatial period in u variable for both ψ and $\tilde{z}$ in equation (2.31). We look for the Stokes wave which has one crest per period. Higher order progressive waves are also possible which have more than one different peak per period Chen & Saffman (1980). However here we consider only Stokes wave. We recall that the spatial period λ is the same in both u and x variables as follows from equation (2.9). In addition, it implies that the phase velocity is the same both in u and x variables so that the Stokes wave has the moving surface $y = \eta(x - ct)$ and the velocity potential $\psi = \psi(x - ct)$ in physical spatial variables (x, y) with the same value of c as in equations (2.31). The Stokes solution requires $y(u)$ to be the even function while $\tilde{x}(u)$ needs to be the odd function which ensures that $y = \eta(x - ct)$ is the even function.

It follows from (2.10) and (2.31) (corresponding to substitution $\frac{\partial}{\partial t} \to -c\frac{\partial}{\partial u}$ for y and ψ and $\frac{\partial x}{\partial t} \to -c\frac{\partial \tilde{x}}{\partial u}$) that $\hat{H}\psi_u = cy_u$ and then excluding ψ from (2.11) we obtain that

$$-c^2 y_u + g y y_u + g\hat{H}[y(1 + \tilde{x}_u)] = 0. \tag{2.32}$$

We now apply $\hat{H}$ to (2.32), use (2.29) to obtain a closed expression for y, and introduce the operator $\hat{k} \equiv -\partial_u \hat{H} = \sqrt{-\nabla^2}$ which results in the following expression

$$\hat{L}_0 y \equiv \left(c^2\hat{k} - 1\right) y - \left(\frac{\hat{k}y^2}{2} + y\hat{k}y\right) = 0, \tag{2.33}$$

where we made all quantities dimensionless by the following scaling transform $u \to u\lambda/2\pi$, $x \to x\lambda/2\pi$, $y \to y\lambda/2\pi$ and c is scaled by c_0 as follows $c \to c\,c_0$, where $c_0 = \sqrt{g/k_0}$ is the phase speed of linear gravity wave with the wavenumber $k_0 = 2\pi/\lambda$. In these scaled units the period of ψ and $\tilde{z}$ is 2π. Our new operator $\hat{k}$ in Fourier space acts as multiplication operator, qualitatively similar to $\hat{H}$: $(\hat{k}f)_k = kf_k$.

3. Numerical simulation of Stokes wave

We solve (2.33) numerically to find $y(u)$ by two different methods each of them beneficial for different range of the parameter H/λ. For both methods $y(u)$ was expanded in cosine Fourier series and the operator $\hat{k}$ was evaluated numerically using Fast Fourier Transform (FFT). A uniform grid with M points was used for the discretization of $-\pi \leqslant u < \pi$. A first method is inspired by a Petviashvili method (Petviashvili 1976) which was originally proposed to find solitons in nonlinear Schrödinger (NLS) equation as well as it was adapted for nonlocal NLS-type equations, see e.g. Lushnikov (2001). We used a version generalized Petviashvili method (GPM) (Lakoba & Yang 2007; Pelinovsky & Stepanyants 2004) adjusted to Stokes wave as described in Dyachenko *et al.* (2013). In practice this method allowed to find high precision solutions up to $H/\lambda \lesssim 0.1388$. The performance of that method for larger values of H/λ was limited by the decrease of the speed of numerical convergence.

3.1. *Newton CG and Newton CR methods*

For larger H/λ we used a second method which is the Newton Conjugate Gradient (Newton-CG) method proposed by Yang (2009, 2010). The idea behind the Newton-CG method is simple and aesthetic: first, linearize (2.33) about the current approximation y_n, assuming that the exact solution can be written as a sum of current approximation and a correction $y = y_n + \delta y_n$: $\hat{L}_0 y = 0$. Then $\hat{L}_0 y_n + \hat{L}_1 \delta y_n \simeq 0$, where $\hat{L}_1 = -\hat{M}\delta y_n - \left(\hat{k}(y_n \delta y_n) + y_n \hat{k}\delta y_n + \delta y_n \hat{k} y_n\right)$ is the linearization of $\hat{L}_0$ around the current approximation y_n and $\hat{M} \equiv -c^2\hat{k} + 1$. Second, solve the resulting linear system $\hat{L}_1 \delta y_n = -\hat{L}_0 y_n$ for δy_n with one of standard numerical methods, in our case it was either Conjugate Gradient (CG) method (Hestenes & Stiefel 1952) or Conjugate Residual (CR) method (Luenberger 1970) to obtain next approximation $y_{n+1} = y_n + \delta y$. It should be noted that monotonic convergence of CG or CR methods is proven only for positive definite (semidefinite for CR) operators, while in our case $\hat{L}_1$ is indefinite. Nevertheless, both methods were converging (although generally nonmonotonically) to the solutions, and convergence was much faster than using GPM.

Newton-CG/CR methods can be written in either Fourier space, or in physical space. We considered both cases, however Newton-CG/CR methods in Fourier space require four fast Fourier transforms per CG/CR step, while in physical space it requires at least six. For both cases CG and CR we used $\hat{M}$ as a preconditioner.

We found that the region of convergence of the Newton-CG/CR methods to nontrivial physical solution (2.33) is relatively (with respect to GPM) narrow and requires an initial guess y_0 to be quite close to the exact solution y. In practice we first run GPM and then choose y_0 for Newton-CG/CR methods as the last available iterate of GPM.

Because most of our interest was in getting dependence of characteristics of Stokes waves on the wave height and the only parameter in equation (2.33) is velocity of propagation c, we were calculating waves changing continuously the parameter c and using results of computations with previous values of c as initial condition y_0 for the Newton CG/CR iterations. Due to this approach Newton-CG/CR methods converge to the nontrivial solution in all cases provided we additionally used the numerical procedure described below in Section 3.2.

3.2. *Stokes wave velocity as a function of steepness*

Results of multiple simulations of Stokes wave are shown in Figure 2, where the wave velocity c is shown as a function of the dimensionless wave height H/λ. This function is nonmonotonic which is in agreement with previous simulations (e.g. Schwartz (1974);

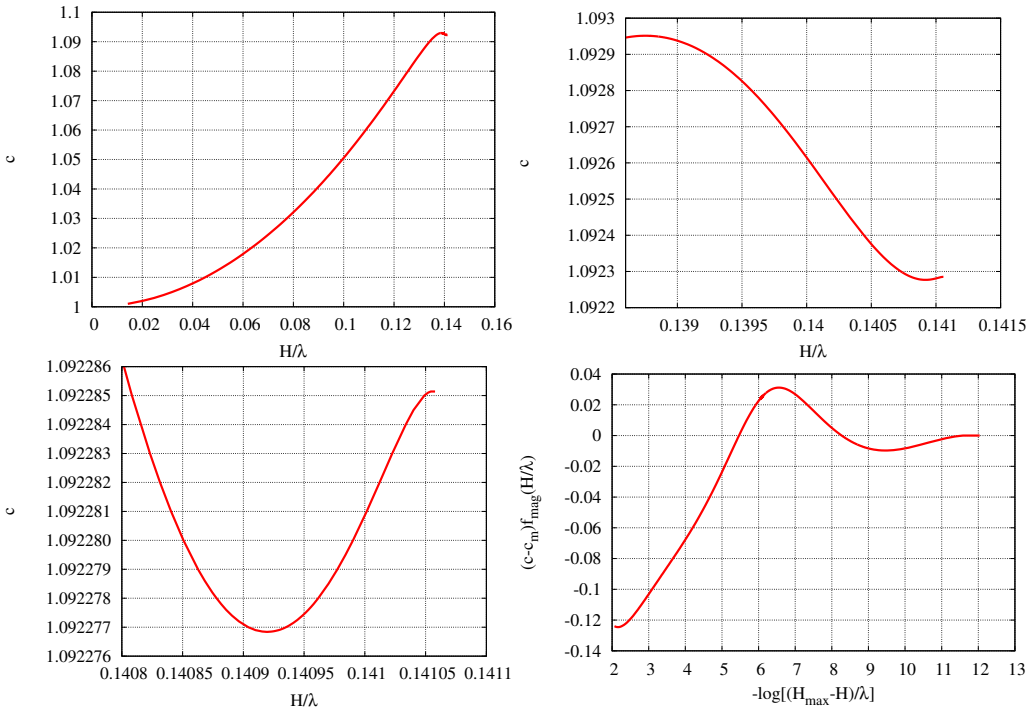


FIGURE 2. Oscillations of dimensionless velocity of Stokes wave propagation as function of steepness obtained from simulations. First three plots from left to right and from top to bottom have increasing zoom both in vertical and horizontal axes to focus on oscillations. In the lower right corner a plot is scaled by a magnification function $f_{mag}(H/\lambda) = 1/(30(H_{max}-H)/\lambda)^{1.15}+1$ to show all simulation data in a single graph while stressing obtained oscillations.

Williams (1981, 1985)) and theoretical analysis (Longuet-Higgins & Fox (1977, 1978)) which predicted an infinite number of oscillations.

We were able to resolve with quadruple precision two oscillations (two maxima and two minima) of the propagation velocity as a function of H/λ. These oscillations represent a challenge for simulation, because propagation velocity is the only parameter in the equation (2.33). Then it is impossible even to go over the first maximum by changing continuously velocity of propagation c. This is because after the maximum is reached, we has to start decreasing the parameter c. But decreasing of c causes iterations to converge to the less steep solution on the left from the maximum (which we already obtained on previous steps), instead of steeper solutions to the right from the maximum.

In order to resolve this issue we used the following approach. Assume that the singularity of $\tilde{z}$ closest to real axis in w complex plane is the branch point

$$\tilde{z} \simeq c_1(w - \mathrm{i}v_c)^\beta \tag{3.1}$$

for $w \to \mathrm{i}v_c$, where c_1 is the complex constant, $v_c > 0$ and β are real constants. By the periodicity in u, similar branch points are located at $w = \mathrm{i}v_c + 2\pi n$, $n = \pm 1, \pm 2, \ldots$ (recall that that we already switched to the dimensionless coordinates). We expand $\tilde{z}(u)$

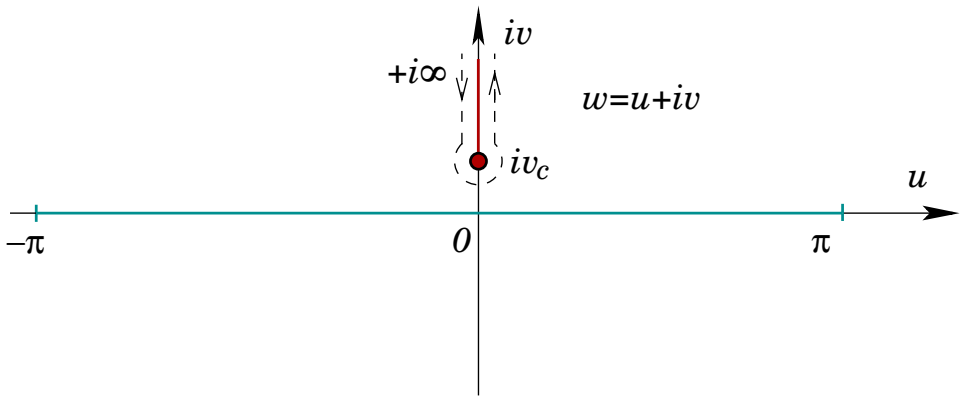


FIGURE 3. Schematic of contour in the $\mathbb{C}^+$ which allows to determine distance v_c from the branch cut to the real axis.

into Fourier series $\tilde{z}(u) = \sum_{-\infty}^{k=0} \hat{\tilde{z}}_k \exp(\mathrm{i}ku)$, where

$$\hat{\tilde{z}}_k = \frac{1}{2\pi} \int_{-\pi}^{\pi} \tilde{z}(u) \mathrm{e}^{-\mathrm{i}ku} \mathrm{d}u \tag{3.2}$$

are Fourier coefficients and the sum is taken over nonpositive integer values of k which ensures both 2π-periodicity of $\tilde{z}(u)$ and analyticity of $\tilde{z}(w)$ in $\mathbb{C}^-$. We evaluate (3.2) in the limit $k \to -\infty$ by moving the integration contour from the line $-\pi < u < \pi$ into $\mathbb{C}^+$ until it hits the lowest branch point (3.1) so it goes around branch point and continues straight upwards about both sides of the corresponding branch cut as shown by the dashed line in right panel of Fig. 3. Here we assume that branch cut is a straight line connecting $w = \mathrm{i}v_c$ and $+\mathrm{i}\infty$. Then the asymptotic of $|\hat{\tilde{z}}_k|$ is given by

$$|\hat{\tilde{z}}_k| \propto |k|^{-1-\beta} e^{-|k|v_c}, \quad k \to -\infty. \tag{3.3}$$

This approach was used in our previous work (Dyachenko *et al.* 2013) to evaluate distance v_c of the lowest singularity to the real line. Now our key idea is to push artificially the singularity $w = iv_c$ toward the real line, thus increasing H/λ. It follows from expression (3.3) that to decrease v_c we can multiply Fourier coefficients of the previously obtained Stokes wave solution $\hat{\tilde{z}}_k$ by $\exp(\alpha k)$, where the numerical parameter α is chosen such that $0 < \alpha \ll v_c$. The result of this multiplication $\hat{\tilde{z}}_k \exp(\alpha k)$ is not a Stokes wave solution anymore, but it has higher steepness and not very distinct from the Stokes wave solution if α is small enough. After that modification we slightly decrease c from previous value and allow iterations of Section 3.1 to converge starting from $\hat{\tilde{z}}_k \exp(\alpha k)$ as zero iteration. As we expected, iterations then converge to the solution on the right from the maximum. This procedure allowed us to resolve both maxima and one nontrivial minimum of c as a function of H/λ as summarized in Fig. 2.

3.3. *Recovering v_c from the Fourier spectrum of Stokes wave*

To obtain the location of the branch point $w = iv_c$ with good precision one has to go beyond the leading order asymptotic (3.3). Next order corrections to the integral (3.2) for $\beta = 1/2$ have the following form

$$|\hat{\tilde{z}}_k| \simeq \left(c_1 |k|^{-3/2} + c_2 |k|^{-5/2} + c_3 |k|^{-7/2} + c_4 |k|^{-9/2} + \dots \right) e^{-|k|v_c}, \quad k \to -\infty, \tag{3.4}$$

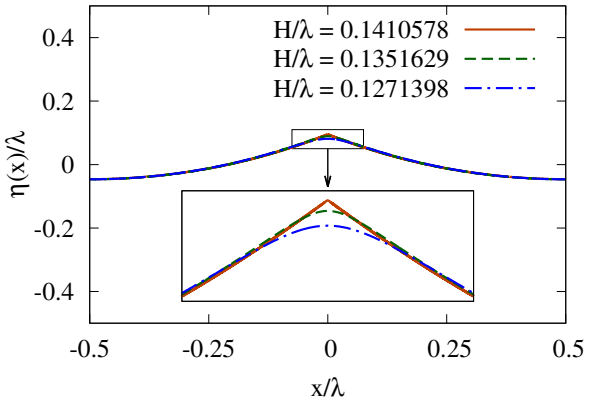


FIGURE 4. Stokes wave with $c = 1.082$ (blue dash-dotted line), $c = 1.091$ (green dashed line) and $c = 1.0922851405$ (dark orange solid line). Corresponding values of H/λ are given in the legend. Inset shows zoom-in into small values of x/λ near a wave crest.

where we took into account the expansion of $\tilde{z}(w)$ in half-integer powers $(w-\mathrm{i}v_c)^{1/2+n}$, $n = 0, 1, 2, \ldots$ beyond the leading order term (3.1).

The numerically obtained spectrum $|\hat{\tilde{z}}_k|$ of Stokes wave was fitted to the expansion (3.4) in order to recover v_c and coefficients $c_1,\ c_2,\ c_3, \ldots$. The highest accuracy in recovering v_c was achieved when the middle of spectrum $k \sim k_{max}/2$ was used for that fit, there $k_{max} = M/2$ is the highest Fourier harmonic used in simulations. $k_{max}/2$ represent a compromise between the highest desired values of k to be as close as possible to asymptotic regime $k \to \infty$ and the loss of numerical precision for $k \to k_{max}$. We estimated the accuracy of the fit by varying values of k used for fitting as well as changing the number of terms in the expansion (3.4). Typically we used 4 terms in (3.4). Section 4.3 discusses the comparison of the accuracy of the obtained results with the other methods we used to find v_c.

3.4. *Highest wave obtained*

We calculated $\tilde{z}(u)$ with high accuracy for different values of H/λ using computations in quad precision (32 digits). Such high precision is necessary to reveal the structure of singularities in $\mathbb{C}^+$. Fig. 4 shows spatial profiles of Stokes waves for several values of H/λ in physical variables (x, y). The Stokes wave quickly approaches the profile of limiting wave except a small neighborhood of the crest.

As it was shown in the previous paper Dyachenko *et al.* (2013), tails of the spectra have asymptotic behavior corresponding to $\beta = 1/2$ in (3.3), which means that we have square root branch cut singularity in $\mathbb{C}^+$ all the time. This is consistent with theoretical predictions by Grant (1973) and Tanveer (1991).

The number of Fourier modes $M \equiv 2k_{max}$ which we used in Fast Fourier Transform (in simulations we expand $y(u)$ in cosine Fourier series to speed up simulations and to be memory efficient) for each value H/λ increases quickly with the increase of H as v_c decreases. E.g., for $H/\lambda = 0.0994457$ it was more than enough to use 256 modes while for the largest wave height

$$H^{num}_{max}/\lambda = 0.14105777885488320816492860225695 6 \tag{3.5}$$

achieved in simulations we used $M = 2^{27} \approx 134 \times 10^6$ modes. Due to such high number of modes, the precision of value (3.5) decreases by round-off errors in approxi-

mately $M^{1/2}$ times, i.e. in ~ 4 digits. This extreme case has $c = 1.0922851405$ and $v_c = 5.93824419892803271779 \times 10^{-7}$. These numbers are the moderate extension of our previous work Dyachenko *et al.* (2013) by pushing down a lowest value of v_c more than twice. Further decrease of the numerical values of v_c can be achieved by both subtracting the leading order singularity (3.1) from the numerical solution and using the nonuniform numerical grid in u which concentrates near $u = 0$. These numerical approaches are however beyond the scope of this papers.

Before our work Dyachenko *et al.* (2013), the numerical estimates of H_{max} were found by Williams (1985) as $H_{max}^{Williams}/\lambda = 0.141063$ and Gandzha & Lukomsky (2007) $H_{max}^{GL}/\lambda = 0.14106348398$. The other commonly used but less precise estimate is $H_{max}^{Schwartz}/\lambda = 0.1412$ (Schwartz 1974). It was shown in Dyachenko *et al.* (2013) that numerical values of v_c in the limit $(H_{max} - H)/\lambda \ll 0$ was fitted to the scaling law (1.1) with

$$H_{max}/\lambda = 0.1410633 \pm 4 \cdot 10^{-7}. \tag{3.6}$$

The mean-square error for δ in (1.1) is $\simeq 0.04$ which offers the exact value $\delta = 3/2$ as a probable candidate for (1.1). The estimate (3.6) suggests that the previous estimate $H_{max}^{Williams}$ is more accurate than $H_{max}^{Schwartz}$. Also H_{max}^{GL} is within the accuracy of the estimate (3.6). However, H_{max}^{GL} is obtained in Ref. Gandzha & Lukomsky (2007) from the Michell's expansion (Michell 1893) of the limiting Stokes wave which ignores the expansion in powers of the irrational number $\mu = 1.46934574\ldots$ Existence of that expansion beyond the Stokes power law $u^{2/3}$ was established by Grant (1973). Lack of resolving that expansion suggests that H_{max}^{GL} does not have a well controlled accuracy. In contrast, our numerical results are based on Fourier series for non-limiting Stokes wave which has well-controlled precision. The difference between (3.6) and the new lower boundary estimate (3.5) of the largest H is $\simeq 0.004\%$.

4. Padé approximation of Stokes wave

4.1. *Additional conformal transformation and spectral convergence of Padé approximation*

To analyze the structure of singularities of Stokes wave we perform an additional conformal transformation between the complex plane $w = u + \mathrm{i}v$ and the complex plane for the new variable

$$\zeta = \tan\left(\frac{w}{2}\right). \tag{4.1}$$

Equation (4.1) maps the strip $-\pi < Re(w) < \pi$ into the complex ζ plane. In particular, the line segment $-\pi < w < \pi$ of the real line $w = u$ maps into the real line $(-\infty, \infty)$ in the complex plane ζ as shown in Fig. 5. Vertical half-lines $w = \pm\pi + \mathrm{i}v$, $0 < v < \infty$ are mapped into a branch cut $\mathrm{i} < \zeta < \mathrm{i}\infty$. In a similar way, vertical half-lines $w = \pm\pi + \mathrm{i}v$, $-\infty < v < 0$ are mapped into a branch cut $-\mathrm{i}\infty < \zeta < \mathrm{i}$. However, $2\pi-$periodicity of $\tilde{z}(w)$ (2.9) allows to ignore these two branch cuts because $\tilde{z}(w)$ is continuous across them. Complex infinities $w = \pm\mathrm{i}\infty$ are mapped into $\zeta = \pm\mathrm{i}$. An unbounded interval $[\mathrm{i}v_c, \mathrm{i}\infty)$, $v_c > 0$ is mapped into a finite interval $[\mathrm{i}\chi_c, \mathrm{i})$ with

$$\chi_c = \tanh\frac{v_c}{2}. \tag{4.2}$$

The mapping (4.1) is different from the commonly used (see e.g. Schwartz (1974); Tanveer (1991); Williams (1981)) mapping $\zeta = \exp(-\mathrm{i}w)$ (maps the strip $-\pi \leqslant Re(w) < \pi$ into the unit circle). The advantage of using the mapping (4.1) is the compactness of the

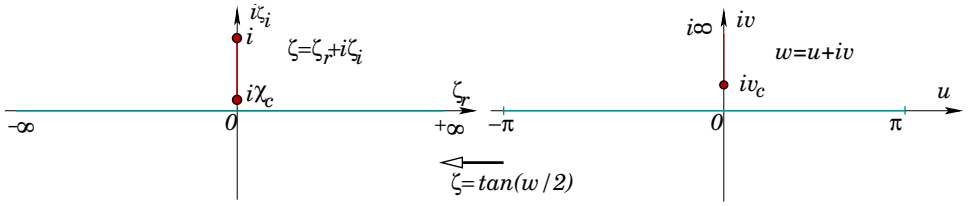


FIGURE 5. Schematic of a second conformal map between the periodic domain in w-plane (right panel) into $\zeta = \tan(w/2)$-plane. Another useful property of this map is representation of 2π-periodic branch cut from $\mathrm{i}v_c$ to $\mathrm{i}\infty$ as a finite length cut from $\chi_c = \tan(\mathrm{i}v_c/2)$ to i.

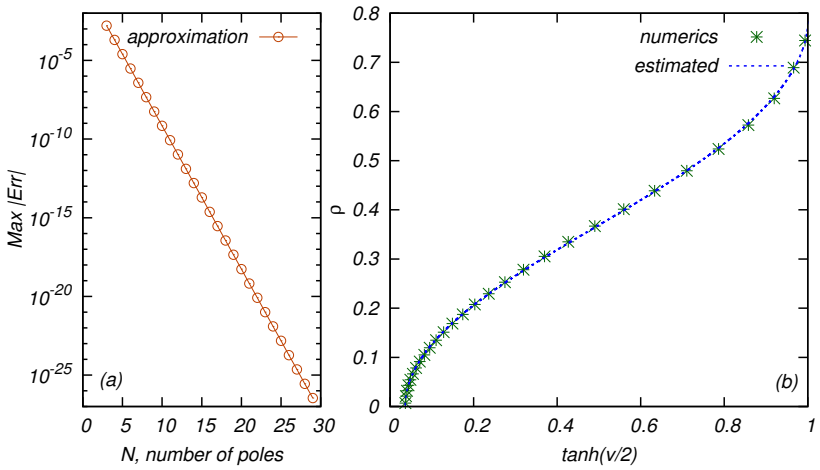


FIGURE 6. (a) An exponential decay of error in Padé approximation of Stokes for $H/\lambda = 0.12551024766621203351189812590805 3$ as a function of the number of poles N. (b) The density $\rho(\chi)$ on the branch cut sampled at $\zeta_k = \mathrm{i}\chi_k \equiv \mathrm{i}\tanh\left(\frac{v_k}{2}\right)$, $k = 1, , \ldots, N$, obtained from the Padé approximation of Stokes wave from(a) with $N = 29$ (green stars). Blue dotted line is the estimated profile of $\rho(\chi)$ for the same Stokes wave in the continuous limit of $N \to \infty$.

interval $(\mathrm{i}\chi_c, \mathrm{i})$ as mapped from the infinite interval $(\mathrm{i}v_c, \mathrm{i}\infty)$. In contrast, the mapping to the circle leaves the interval $(\mathrm{i}v_c, \mathrm{i}\infty)$ infinite in ζ plane.

We use Alpert-Greengard-Hagstrom (AGH) algorithm (Alpert *et al.* 2000; Lau 2004) to approximate the Stokes wave $\tilde{z}(\zeta)$ at the real line $\mathrm{Re}(\zeta) = \zeta$ by a set a poles in the complex ζ plane. Approximation by a set of poles is a particular case of Padé approximation by rational functions $\frac{P(\zeta)}{Q(\zeta)}$, where $P(\zeta)$ and $Q(\zeta)$ are polynomials. Zeros of $Q(\zeta)$ give the location of poles. Looking at complex values of ζ in the rational function $\frac{P(\zeta)}{Q(\zeta)}$ provides the analytical continuation of $\tilde{z}(\zeta)$ into the complex ζ plane. Usually Padé approximation is numerically unstable because of the pairs of spurious zeros and poles appear in finite precision arithmetics. These doublets correspond to positions of zeros of $P(\zeta)$ and $Q(\zeta)$ which are nearly cancel each other. In our practical realizations, AGH algorithm avoids the numerical instability of the Padé approximation until the number of poles N increases to reach the accuracy corresponding to the round-off error in the numerical approximation of $\tilde{z}(u)$. If the analytical continuation of $\tilde{z}(u)$ into $w \in \mathbb{C}$ has a branch cut, the AGH algorithm places poles along the branch cut. AGH algorithm is outlined in Appendix B.

We applied AGH algorithm for $\tilde{z}(\zeta)$ at the real line $\mathrm{Re}(\zeta) = \zeta$, where $\tilde{z}(\zeta)$ is obtained from simulations described in Section 3. Increasing N we observed the exponential con-

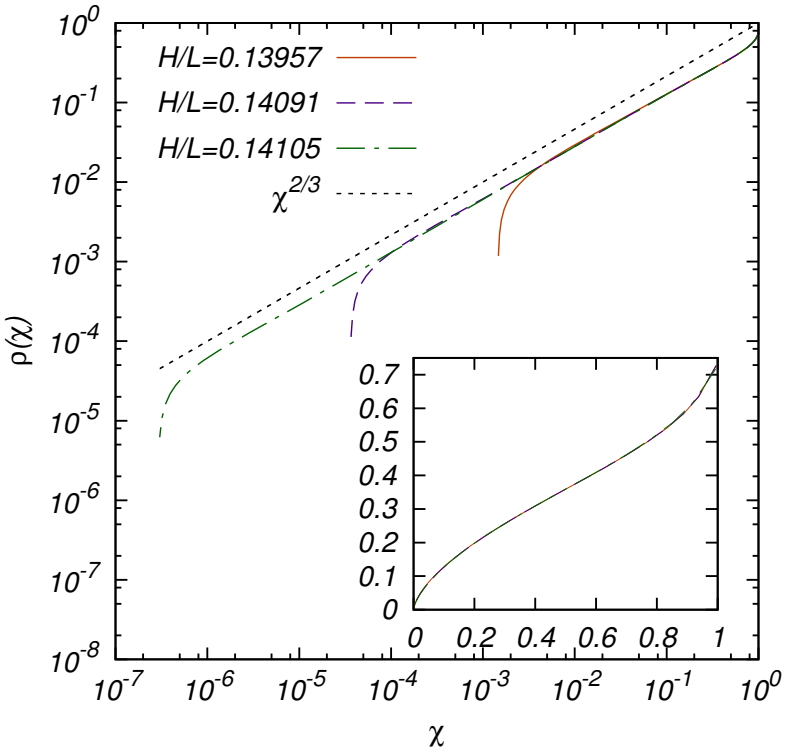


FIGURE 7. The density $\rho(\chi)$ for three different Stokes waves in log-log scale. A straight dashed line shows $\chi^{2/3}$ scaling law which corresponds to the limiting Stokes wave. Insert shows $\rho(\chi)$ in linear scale for the same three Stokes wave which are visually almost indistinguishable.

vergence of Padé approximation $z(\zeta)_{pade}$ to $\tilde{z}(\zeta)$ as

$$err_\infty \propto e^{-p(v_c)N}, \tag{4.3}$$

where $err_\infty \equiv \max\limits_{-\infty<\zeta<\infty} |\tilde{z}(\zeta) - \tilde{z}(\zeta)_{pade}|$ is the error in infinity (maximum) norm. An example of the exponential convergence is shown in Figure 6a for a particular Stokes wave. Here $p(v_c)$ is the function of v_c but is independent on N. We found that with high precision

$$p(v_c) \propto v_c^{1/6}. \tag{4.4}$$

AGH algorithm is looking for poles in the entire complex plane ζ. All the encountered poles for Stokes wave were found on the interval of imaginary axis along the interval $[\mathrm{i}\chi_c, \mathrm{i})$, where χ_c is determined numerically as in Section 3.

Equations (4.3) and (4.4) demonstrate excellent performance of Padé approximation. E.g., decreasing v_c by six order required in our simulations only 10-fold increase of N as detailed in Appendix C. It suggests that numerical method which solves Stokes wave equation (2.33) directly in terms of Padé approximants might be superior to Fourier methods including numerical approaches mentioned in Section 3.3. This topic is however beyond the scope of this paper.

It is rather straightforward to distinguish in AGH algorithm poles from branch cuts. If both poles and branch cuts would be present in $\tilde{z}(\zeta)$ then increasing N one observes that some poles of Padé approximation are not moving and their complex residues remain approximately the same. These correspond to poles of $\tilde{z}(\zeta)$. Such behavior occurs for

test problems when we artificially added extra poles to $\tilde{z}(\zeta)$. Other poles of Padé approximation are moving with the increase of N and their complex residues are changing. These poles mark the spatial location of branch cuts of $\tilde{z}(\zeta)$. The density of poles along each branch cut is increasing with the increase of N. If the jump of $\tilde{z}(\zeta)$ at branch cut is continuous along it then we expect to see the convergence of density of poles with the increase of N. All this is valid until err_∞ decreases down to the level of round-off error at which $\tilde{z}(\zeta)$ was determined. Further increase of N would result in the appearance of spurious poles at random positions of ζ plane with the magnitudes of complex residues at the level of round off error ($\sim 10^{-32}$ for $z(\zeta)$ found with quad precision in Section 3).

Using $\tilde{z}(\zeta)$ obtained by the method of Section 3, we found a single branch cut $[\mathrm{i}\chi_c, \mathrm{i})$ but no poles in Stokes wave. It means that in complex w plane we have one branch cut per spatial period 2π located at $(2\pi n + \mathrm{i}v_c, 2\pi n + \mathrm{i}\infty)$, $n \in \mathbb{N}$.

We parametrize that branch cut as follows

$$\tilde{z}(\zeta) = \mathrm{i}y_0 + \int\limits_{\chi_c}^{1} \frac{\rho(\chi')\mathrm{d}\chi'}{\zeta - \mathrm{i}\chi'}, \tag{4.5}$$

where $\rho(\chi)$ is the density along branch cut. That density is related to the jump of $\tilde{z}(\zeta)$ at branch cut as explained in Section 5.1. The constant y_0 is determined by the value of $\tilde{z}(\zeta)|_{\zeta=\infty} = \tilde{z}(w)|_{w=\pi}$. This constant has a zero imaginary part, $\mathrm{Im}(y_0) = 0$, because $\tilde{x}(w)|_{w=\pi/2} = 0$ as given by the equation (2.9).

The Padé approximation represents equation (4.5) as follows

$$\tilde{z}(\zeta) = \mathrm{i}y_0 + \int\limits_{\chi_c}^{1} \frac{\rho(\chi')\mathrm{d}\chi'}{\zeta - \mathrm{i}\chi'} \simeq \mathrm{i}y_0 + \sum_{n=1}^{N} \frac{\gamma_n}{\zeta - \mathrm{i}\chi_n}, \tag{4.6}$$

where the numerical values of the pole positions χ_n and the complex residues γ_n ($n = 1, \ldots, N$) are obtained from AGH algorithm.

4.2. *Recovering jump along branch cut*

We recover $\rho(\chi)$ from equation (4.6) as follows. Assume that we approximate the integral in equation (4.5) by the trapezoidal rule

$$\begin{aligned}\int\limits_{\chi_c}^{1} \frac{\rho(\chi')\mathrm{d}\chi'}{\zeta - \mathrm{i}\chi'} \simeq & \frac{\chi_2 - \chi_1}{2}\frac{\rho_1}{\zeta - \mathrm{i}\chi_1} \\ & + \sum_{n=2}^{N-1} \frac{\chi_{n+1} - \chi_{n-1}}{2}\frac{\rho_n}{\zeta - \mathrm{i}\chi_n} + \frac{\chi_N - \chi_{N-1}}{2}\frac{\rho_N}{\zeta - \mathrm{i}\chi_N}.\end{aligned} \tag{4.7}$$

A comparison of equations (4.6) and (4.7) suggests the approximation $\rho_{n,N}$ of the density $\rho(\chi_n)$ on the discrete grid χ_n, $n = 1, \ldots, N$ as follows

$$\rho(\chi_n) \simeq \rho_{n,N} = \frac{2\gamma_n}{\chi_{n+1} - \chi_{n-1}} \text{ for } n = 2, \ldots, N-1, \tag{4.8a}$$

$$\rho(\chi_1) \simeq \rho_{1,N} = \frac{2\gamma_1}{\chi_2 - \chi_1};\ \rho(\chi_N) \simeq \rho_{N,N} = \frac{2\gamma_N}{\chi_N - \chi_{N-1}}. \tag{4.8b}$$

A convergence of $\rho_{n,N}$ to the continuous limit $\rho(\chi_n)$ as N increases is quadratic with the error scaling $\propto \frac{1}{N^2}$ for χ away from boundaries $\chi = \chi_c$ and $\chi = 1$. Near these boundaries we cannot apply the trapezoidal rule and have to resort to less accurate

estimates given by the equation (4.8*b*). Figure 8 demonstrates this $\propto \frac{1}{N^2}$ convergence of the Padé approximation to the continuous limit. Figure 6b shows the particular example of $\rho(\chi)$ (shown by solid line solid line) compared with $\rho_{n,N}$ (shown by stars) for $N = 29$. We believe that the convergence of ρ_n to the continuous value $\rho(\chi)$ as $N \to \infty$ and absence of other poles outside of $[\mathrm{i}\chi_c, \mathrm{i}]$ provide a numerical proof that the only singularity of $\tilde{z}(\zeta)$ are the branch points $\mathrm{i}\chi_c$ and i connected by the branch cut $\zeta \in [\mathrm{i}\chi_c, \mathrm{i}]$.

At $\chi = \chi_c$ the function $\rho(\chi)$ has a square root singularity as given below by equation (4.13). This singularity additionally reduces the accuracy of the approximation (4.8*b*) for $\rho_{1,N}$ which is based on Taylor series. To significantly improve numerical accuracy of $\rho_{1,N}$ we assume that ρ has the following square root dependence in the vicinity of χ_c:

$$\rho_{approx}(\chi) = A\sqrt{\chi - \chi_c}. \tag{4.9}$$

Here the values of the parameters A and χ_c are determined from two interior points $(\chi_2, \rho_{2,N})$ and $(\chi_3, \rho_{3,N})$ found via the trapezoid rule (4.8*a*). We assume that $\rho_{approx}(\chi_2) = \rho_{2,N}$ and $\rho_{approx}(\chi_3) = \rho_{3,N}$ which gives that

$$A = \left(\frac{\rho_{3,N}^2 - \rho_{2,N}^2}{\chi_3 - \chi_2}\right)^{1/2}, \qquad \chi_c = \frac{\rho_{3,N}^2\chi_2 - \rho_{2,N}^2\chi_3}{\rho_{3,N}^2 - \rho_{2,N}^2}. \tag{4.10}$$

Using equations (4.9) and (4.10) for $\chi = \chi_1$ we obtain the numerically accurate approximation that

$$\rho_{1,N} = \left(\frac{(\chi_3 - \chi_1)\rho_{2,N}^2 - (\chi_2 - \chi_1)\rho_{3,N}^2}{\chi_3 - \chi_2}\right)^{1/2}, \tag{4.11}$$

where $\rho_{2,N}$ and $\rho_{3,N}$ are given by equation (4.8*a*).

At $\chi = 1$ the function $\rho(\chi)$ also has singularity and respectively numerical value of $\rho_{N,N}$ from (4.8*b*) is not very accurate. To improve that accuracy we use that $\rho(1) = 1$ as found in Part II. Then using the trapezoidal rule we obtain much more accurate expression that

$$\rho(\chi_N) \simeq \rho_{N,N} = \frac{2\gamma_N}{1 - \chi_{N-1}}. \tag{4.12}$$

Figure 7 shows the density $\rho(\chi)$ for three different Stokes waves in log-log scaling. It is also seen that inside the branch cut and for small $\chi_c \ll 1$, the density $\rho(\chi)$ scales as $\chi^{2/3}$ which corresponds to the limiting Stokes wave. A deviation from that scaling occurs near $\chi = \chi_c$ and $\chi = 1$.

Classical Markov's theorem (Markoff 1895) proves pointwise convergence of the diagonal Padé approximants $[N/N]_f$ of the function f of the type (4.5) with $\rho(\chi) \geqslant 0$ in the limit $N \to \infty$ for $\zeta \in \mathbb{C} \setminus [\mathrm{i}\chi_c, \mathrm{i}]$. Here the diagonal Padé approximation $[N/N]_f$ of the function f means that both polynomials $P(\zeta)$ and $Q(\zeta)$ has the same order N which is natural for the discretization (4.6). More general Padé approximants of the function f are $[N/M]_f$, where N and M are the orders of the polynomials $P(\zeta)$ and $Q(\zeta)$, respectively. Theorem of de Montessus de Ballore (1902) ensures pointwise convergence of $[N/M]_f \to f$ for $N \to \infty$ with fixed M in the disk $|\zeta| < R$ if f the meromorphic function in that disk with exactly M poles (counted according to their multiplicity). However, the diagonal Padé approximations of the meromorphic function f generally fails to provide uniform convergence with the known counterexamples given by Buslaev (2001); Lubinsky (2003). Nuttall (1970) showed that instead the diagonal Padé approximants of meromorphic function for $N \to \infty$ have a weaker convergence in logarithmic

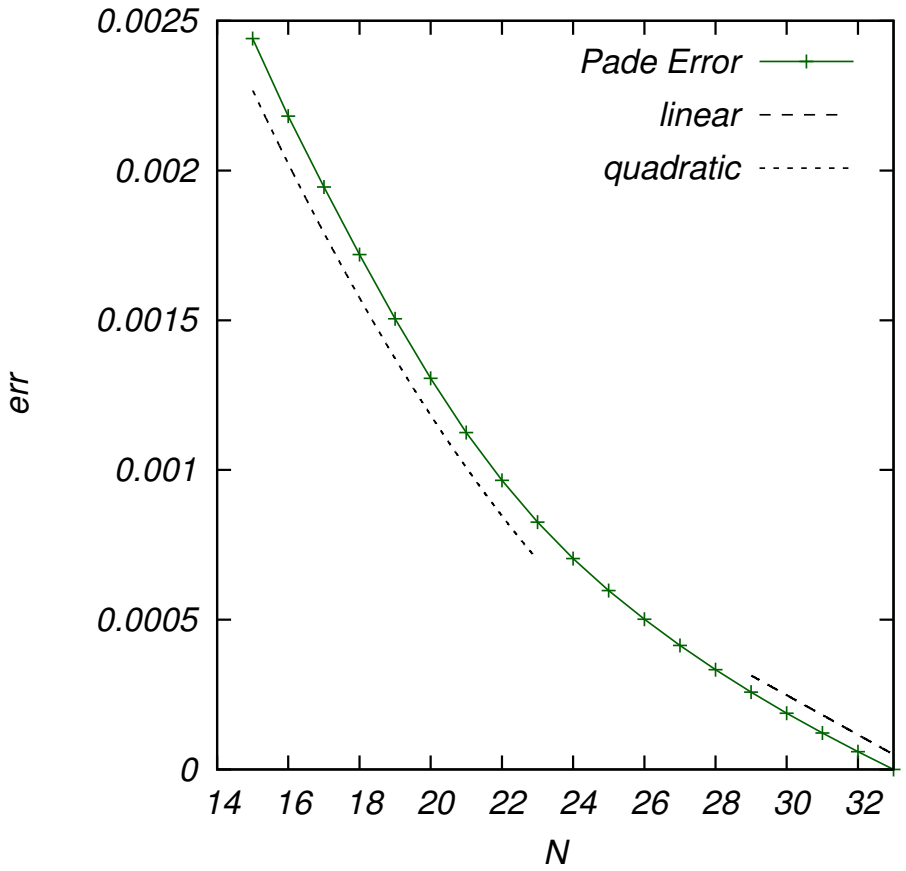


FIGURE 8. Error between Padé approximation with N poles and the continuous limit for $\rho(\chi)$ for Stokes wave with $H/\lambda = 0.12551024766621203511898125908053$. It is seen that the error $\propto \frac{1}{N^2}$ for large N. To calculate that error we use a spline interpolation for $\rho^2_{n,N}$ with $N = N_{max} = 33$ to construct the approximation of the continuous limit of the square of the density, $\rho^2_{continuous}(\chi)$. After that the error is defined as $\mathrm{err} \equiv \left(\sum_{n=2}^{N-1}[\rho^2_{n,N} - \rho^2_{continuous}(\chi_n)]^2\right)^{1/2}/(N-2)$ for each N, where $\rho_{n,N}$ is given by equation (4.8).

capacity which allows the lack of pointwise convergence along exceptional sets. Gonchar (Gonchar 1973, 1975) extended Markov's theorem on the pointwise convergence of the diagonal Padé approximants to the functions $f + r$, where f is the function of the type (4.5) with $\rho(\chi) > 0$ almost everywhere in $\chi \in [\chi_c, 1]$ and r is the meromorphic function away from branch cut and has no poles at branch cut. Convergence in logarithmic capacity of the diagonal Padé approximants of the analytic function $f(\zeta)$ with a finite number of branch points (this is a more general type than the type (4.5) because these branch points can be located away from a single line) was proven by Stahl (1985*a*,*b*, 1997). That convergence occurs away from certain sets of $\mathbb{C}$ (in some cases these sets are simple arcs). See also Ref. Aptekarev *et al.* (2011) for the recent review. All these results were obtained for Padé approximants based on the Taylor series at a single point in $\mathbb{C}$. Thus these results do not directly apply to AGH algorithm which is based on least squares approximation at multiple points of $\mathbb{C}$. AGH algorithm is also distinct from multipoint Padé approximation (G. A. Baker & Graves-Morris 1996; Saff 1972), where the Taylor

series is interpolated at multiple points in contrast to least squares in AGH algorithm. Padé approximants were also constructed based on least squares in Ref. Gonnet *et al.* (2011) were it was conjectured that least squares-type algorithms might ensure pointwise convergence. That conjecture is consistent with our simulations.

4.3. *Finding a numerical value of a location of branch point $\zeta = i\chi_c$*

There are different ways to find the location of branch point $\zeta = \mathrm{i}\chi_c$ from simulations. First way is based on the decay of Fourier spectrum of $\tilde{z}(\zeta)$ for $n \gg 1$ and is described in Section 3.3. Second way is to find $\rho(\chi_n)$, $n = 1, \ldots, N$ and then determine the point $\rho(\chi_c) = 0$ by the polynomial extrapolation of $\rho(\chi_n)$. First and second ways provide comparable numerical accuracy in our simulations (typically the relative error in χ_c is $\sim 10^{-4}$).

We found however, that better accuracy is achieved in the third way as follows. Consider the formal series

$$\tilde{z}_{ser} = \sum_{j=0}^{\infty} i e^{\mathrm{i}j\pi/4} a_j (\zeta - \mathrm{i}\chi_c)^{j/2} \tag{4.13}$$

in the neighborhood of the branch point $\zeta = \mathrm{i}\chi_c$. The term $ie^{\mathrm{i}j\pi/4}$ in front of the coefficients a_j is chosen for convenience to ensure that coefficients a_j take real values. The radius of convergence of that series is $2\chi_c$ as discussed in Part II. Taking $M = 10 - 20$ terms in that series one can use the nonlinear fit to determine the unknowns χ_c and a_j. Typically we use $N_j = 30 - 40$ points $(u_n, \tilde{z}(u_n))$ such that all values u_n are inside the disk of convergence $|u_n - \mathrm{i}\chi_c| < 2\chi_c$ of the series (4.13). Here values of $\tilde{z}(u_n)$ are taken from simulations of Section 3 with u_n being the numerical grid points closest to $u = 0$. The accuracy of the nonlinear fit is typically $\sim 10^{-10}$ as estimated by varying M and N_M. In Part II we provide much more accurate way of calculating χ_c which is based on the compatibility of the series (4.13) with the equation (2.33) of Stokes wave. In contrast, the above three methods use numerical values of $(u_n, \tilde{z}(u_n))$ obtained as described in Section 3 and do not use the equation (2.33) directly.

5. Stokes wave as an integral over jump at branch cut and the expansion of density ρ near a branch point

5.1. *Jump at branch cut*

Sokhotski-Plemelj theorem (see e.g. Gakhov (1966); Polyanin & Manzhirov (2008)) applied to the equation (4.5) gives

$$\tilde{z}(\mathrm{i}\chi \pm 0) = \mathrm{i}y_0 + \mathrm{p.v.} \int_{\chi_c}^{1} \frac{\rho(\chi')\mathrm{d}\chi'}{\mathrm{i}(\chi - \chi')} \pm \pi\rho(\chi), \;\; \chi_c < \chi < 1. \tag{5.1}$$

Thus the jump of $\tilde{z}(\zeta)$ at branch cut is $-2\pi\rho(\chi)$ for crossing branch cut at $\zeta = \mathrm{i}\chi$ in counterclockwise direction.

5.2. *Stokes wave as the sum of contribution from branch cuts in w complex plane*

Consider a representation of Stokes wave by the density $\tilde{\rho}$ along branch cuts in complex plane w. Because of the 2π-periodicity in u direction we write $z(w)$ as the integral over

periodically located branch cuts,

$$\tilde{z}(w) = z_1 + \int_{v_c}^{\infty} \sum_{n=-\infty}^{\infty} \left(\frac{1}{w + 2\pi n - \mathrm{i}v'} - \frac{1}{b + 2\pi n - \mathrm{i}v'} \right) \tilde{\rho}(v')\mathrm{d}v', \tag{5.2}$$

where z_1 is the complex constant, v_c is related to χ_c by (4.2), a summation over n ensure the periodicity of $\tilde{z}(w)$ along u and we replaced $\rho(\chi)$ by $\tilde{\rho}(v')$ to distinguish it from $\rho(\chi)$ in (4.5). Also we introduced the additional term $-\dfrac{1}{b + 2\pi n - \mathrm{i}v'}$ which is intended to ensure the convergence of the integral. The constant b can be chosen at our convenience. A change of that constant results in the change of z_1.

The sum in (5.2) is then calculated using of the identity

$$\sum_{n=-\infty}^{\infty} \frac{1}{n + a} = \pi \cot \pi a$$

giving

$$\tilde{z}(w) = z_1 + \frac{1}{2} \int_{v_c}^{\infty} \left(\cot \left[\frac{w - \mathrm{i}v'}{2} \right] - \cot \left[\frac{b - \mathrm{i}v'}{2} \right] \right) \tilde{\rho}(v')\mathrm{d}v'. \tag{5.3}$$

Taking the limit $Im(w) \to -\infty$ we obtain from equations (5.3) and (4.5) that

$$\tilde{z}(u - \mathrm{i}\infty) = z_1 + \frac{1}{2} \int_{v_c}^{\infty} \left(i - \cot \left[\frac{b - \mathrm{i}v'}{2} \right] \right) \tilde{\rho}(v')\mathrm{d}v' = iy_0 + \int_{\chi_c}^{1} \frac{\rho(\chi)\mathrm{d}\chi}{-\mathrm{i} - \mathrm{i}\chi}. \tag{5.4}$$

We set

$$\chi = \tanh \frac{v'}{2} \tag{5.5}$$

and

$$\rho(\chi) = \tilde{\rho}(2 \operatorname{arctanh} \chi). \tag{5.6}$$

We also require that $z_1 = \mathrm{i}y_0$ then we find from the equations (5.4), (5.5) and (5.6) that

$$b = \pi. \tag{5.7}$$

Using the trigonometric identity

$$\cot (a - b) = \frac{1 + \tan a \tan b}{\tan a - \tan b}$$

one obtains from (5.3), (5.4), (5.5), (5.6) and (5.7) that

$$\begin{aligned} \tilde{z}(w) &= \mathrm{i}y_0 + \frac{1}{2} \int_{v_c}^{\infty} \left(\frac{\left[1 + \mathrm{i} \tan \frac{w}{2} \tanh \frac{v'}{2} \right]}{\tan \frac{w}{2} - \mathrm{i} \tanh \frac{v'}{2}} - \mathrm{i} \tanh \frac{v'}{2} \right) \tilde{\rho}(v')\mathrm{d}v' \\ &= \mathrm{i}y_0 + \frac{1}{2} \int_{v_c}^{\infty} \left(\frac{1 + \mathrm{i}\zeta\chi}{\zeta - \mathrm{i}\chi} - \mathrm{i}\chi \right) \tilde{\rho}(v')dv' = \mathrm{i}y_0 + \int_{\chi_c}^{1} \frac{\rho(\chi)\mathrm{d}\chi}{\zeta - \mathrm{i}\chi}, \end{aligned} \tag{5.8}$$

i.e. we recovered the equation (4.5) from the equation (5.2).

5.3. *Expansion of $\rho(\chi)$ in powers of $\zeta - i\chi_c$*

Assume that we have the branch cut $(\mathrm{i}\chi_c, \mathrm{i})$ for $z(\zeta)$ in the complex plane of ζ and that the branch point at $\zeta = \mathrm{i}\chi_c$ is of square root type. Then we expand $\rho(\chi)$ in the following series

$$\rho(\chi) = \sum_{n=0}^{\infty} b_{2n+1}(\chi - \chi_c)^{1/2+n}. \tag{5.9}$$

Note that that adding terms of integer powers of $(\zeta - \mathrm{i}\chi_c)$ into the equation (5.9) is not allowed because it would produce logarithmic singularity at $\zeta = \mathrm{i}\chi_c$ through the equation (4.5) which is incompatible with the Stokes wave as was shown in Refs. Grant (1973); Tanveer (1991).

Integrating over χ in (4.5) using (5.9) gives

$$\begin{aligned} f(\zeta) = {} & b_1 \left(2\mathrm{i}\sqrt{1-\chi_c} - 2\mathrm{i}\sqrt{\chi_c + \mathrm{i}\zeta}\, \arctan\left[\frac{\sqrt{1-\chi_c}}{\sqrt{\chi_c+\mathrm{i}\zeta}}\right]\right) \\ & + b_3 \left(\frac{2}{3}\sqrt{1-\chi_c}(\mathrm{i} - 4\mathrm{i}\chi_c + 3\zeta) + 2\mathrm{i}(\chi_c + \mathrm{i}\zeta)^{3/2} \arctan\left[\frac{\sqrt{1-\chi_c}}{\sqrt{\chi_c+\mathrm{i}\zeta}}\right]\right) \\ & + b_5 \left(\frac{2}{15}\sqrt{1-\chi_c}\left(3\mathrm{i} - 11\mathrm{i}\chi_c + 23\mathrm{i}\chi_c^2 + 5\zeta - 35\chi_c\zeta - 15\mathrm{i}\zeta^2\right)\right. \\ & \left. -2\mathrm{i}(\chi_c + \mathrm{i}\zeta)^{5/2} \arctan\left[\frac{\sqrt{1-\chi_c}}{\sqrt{\chi_c+\mathrm{i}\zeta}}\right]\right) + b_7(\ldots) + \ldots \end{aligned} \tag{5.10}$$

A series expansion of (5.10) at $\zeta = \mathrm{i}\chi_c$ and comparison with the series (4.13) result in the relations

$$b_{2j+1} = (-1)^{j+1} a_{2j+1},\ j = 0, 1, 2, \ldots \tag{5.11}$$

Note that the expansion (5.10) provides the relations for b_n with only odd values of n. This is because the series (5.9) is convergent only inside its disk of convergence, $\chi - \chi_c < r$, where r is the radius of convergence. It will be shown in Part II that $r = 2\chi_c$ for $\chi_c < 1/3$. The explicit expression for $\rho(\chi)$ is unknown for $\chi_c + r < \chi < 1$ while $\rho(\chi)$ still contributes to the terms $a_{2j}(\zeta - \mathrm{i}\chi_c)^j,\ j = 0, 1, 2, \ldots$ in the series (4.13).

Thus the expansion (5.9) together with the relations (5.11) provides a convenient tool to work with $\rho(\chi)$ near to $\chi = \chi_c$.

5.4. *Absence of singularities in branch cut beyond the branch points $\zeta = i\chi_c$ and $\zeta = i$.*

A priori one can not exclude existence of singularities inside the branch cut $\zeta \in [\mathrm{i}\chi_c, \mathrm{i}]$ beyond branch points $\zeta = \mathrm{i}\chi_c$ and $\zeta = \mathrm{i}$ at its ends. Existence of such singularities were conjectured in Refs. Grant (1973); Schwartz (1974). To address that possibility we subtracted the expansion (5.10) from the numerical solution of $\tilde{z}(\zeta)$ for Stokes wave. We obtained both $\tilde{z}(\zeta)$ and recovered $\rho(\chi)$ through AGH algorithm using variable precision arithmetics with ~ 200 digits to achieve a high precision in that subtraction. Typically we used Stokes wave of the moderate nonlinearity with $\chi_c \sim 10^{-2}$ to operate with the moderate number of required Fourier harmonics. After that the numerical values of $b_1, b_3, b_5, \ldots$ were recovered from fitting of $\rho(\chi)$ to the expansion (5.9) near $\chi = \chi_c$. Typically we truncated the expansion (5.9) to the first 3 terms b_1, b_3, b_5 which results in the truncated function $f(\zeta)_{truncated}$ in the expansion (5.10). Also χ_c was obtained by the procedures described in Section 4.3. Alternative way to recover b_1, b_3, b_5 is through using the expansion (3.4) was also used but generally gives lower precision.

Next step was to take mth derivative of $\tilde{z}(\zeta) - f(\zeta)_{truncated}$ over ζ numerically and

obtain the Padé approximation for the resulting expression $[\tilde{z}(\zeta) - f(\zeta)_{truncated}]^{(m)}$ resulting in new density $\tilde{\rho}(\chi)$. If any singularity would be present inside the branch cut then it would correspond to singularity in $\tilde{\rho}(\chi)$. However, we did not find any sign of such singularities at least for moderate order of derivative $m = 1, 2, 3$. It suggests that $\zeta = \mathrm{i}\chi_c$ and $\zeta = \mathrm{i}$ are the only singularities in complex ζ plain. This conclusion is in agreement with the results of both Tanveer (1991) and Part II obtained by alternative methods.

6. Conclusion

In this paper we found numerically the Stokes solutions of the primordial Euler equations with free surface for large range of wave heights, including the approach to the limiting Stokes wave. The limiting Stokes wave emerges as the singularity reaches the fluid surface. We found from our high precision simulations (between 32 and more than 200 digits) the Padé approximation of branch cut singularity of Stokes wave. We provided the tables of the Padé approximants for a wide range of Stokes wave steepness. These tables allow to recover Stokes wave with the minimum accuracy 10^{-26}. We show that these Padé approximants quickly converge to the jump at branch cut as the number of poles N increases with the scaling law (4.3),(4.4). We use the series expansion of the jump along branch cuts in half integer powers to recover the square-root singularity at the branch point. We found that there are no more singularities in the finite complex plane beyond one branch point per period. Following Part II is devoted to the analysis of the structure and location of branch points in infinite set of sheets of Riemann surface beyond the physical sheet of Riemann surface considered here.

The authors would like to thank Prof. S. Lau for the introduction to AGH method of Padé approximation and sharing his computer codes which were used at the initial stage of research. Also the authors thank developers of FFTW (Frigo & Johnson 2005) and the whole GNU project (GNU Project 1984-2012) for developing, and supporting this useful and free software. The work of S.D. and A.K. was partially supported by the U.S. National Science Foundation (grant no. OCE 1131791). The work of A.K. and P.L. on the Padé approximation was supported by Russian Science Foundation grant 14-22-00259.

Appendix A. Derivation of dynamical equations

In this Appendix we adapt the work of Dyachenko *et al.* (1996*a*) to the case of the periodic boundary conditions deriving the basic dynamical equations (2.10) and (2.11) for 2D ideal hydrodynamics with free surface in conformal variables. We use similar notations to Dyachenko *et al.* (1996*a*) and provide steps of the derivation skipped in Dyachenko *et al.* (1996*a*).

A.1. *Hamiltonian after conformal map*

It was shown by Zakharov (1968), that the potential flow of an ideal fluid with free surface is the canonical Hamiltonian system with canonical variables η (2.4) and ψ (2.5). Canonical Hamiltonian equations

$$\frac{\partial \eta}{\partial t} = \frac{\delta H}{\delta \psi}, \quad \frac{\partial \psi}{\partial t} = -\frac{\delta H}{\delta \eta}. \tag{A 1}$$

are equivalent to the boundary conditions (2.2) and (2.3). Here H is the Hamiltonian which coincides with the total energy (the sum of the kinetic energy T and the potential

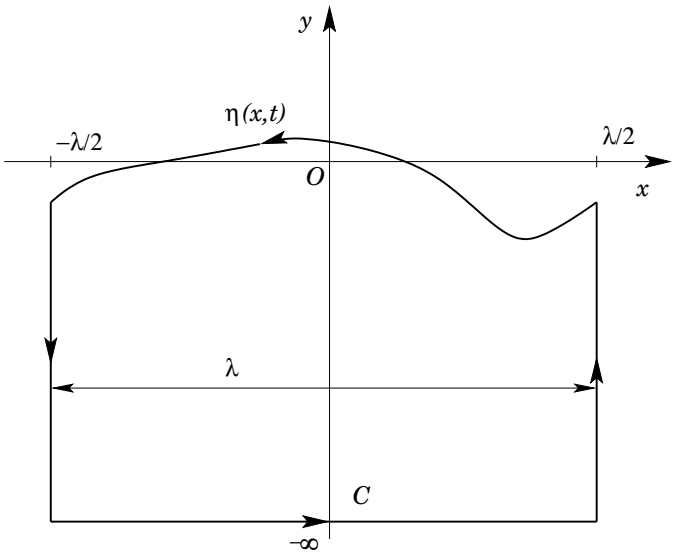


FIGURE 9. A schematic of one period of a wave with a counterclockwise contour of integration for application of Green's theorem.

energy U) per spatial period of wave λ,

$$H = T + U = \frac{1}{2}\int\limits_{-\lambda/2}^{\lambda/2} \mathrm{d}x \int\limits_{-\infty}^{\eta} (\nabla\Phi)^2 \mathrm{d}y + \frac{g}{2}\int\limits_{-\lambda/2}^{\lambda/2} \eta^2 \mathrm{d}x,$$

and without loss of generality the fluid density is set to one. One has to express the kinetic energy

$$T = \frac{1}{2}\int\limits_{-\lambda/2}^{\lambda/2} \mathrm{d}x \int\limits_{-\infty}^{\eta} (\nabla\Phi)^2 \mathrm{d}y \tag{A 2}$$

through the canonical variables η and ψ which generally requires to solve the Laplace equation (2.1) with the boundary conditions (2.2), (2.3), (2.5) and $\Phi(x,y,t)|_{y\to-\infty} = 0$ in the region $-\frac{\lambda}{2} \leqslant x < \frac{\lambda}{2}$, $-\infty < y \leqslant \eta(x,t)$. That region is schematically shown in Figure 9. Using relations

$$\nabla\cdot(\Phi\nabla\Phi) = (\nabla\Phi)^2 + \Phi\nabla^2\Phi, \quad (\nabla\Phi)^2 = \frac{\partial}{\partial x}\left(\Phi\frac{\partial\Phi}{\partial x}\right) + \frac{\partial}{\partial y}\left(\Phi\frac{\partial\Phi}{\partial y}\right),$$

which are valid for the harmonic function Φ (2.1) and applying Green's theorem to the equation (A 2) one obtains that

$$2T = \int\limits_{-\lambda/2}^{\lambda/2}\int\limits_{-\infty}^{\eta} \left\{\frac{\partial}{\partial x}\left(\Phi\frac{\partial\Phi}{\partial x}\right) + \frac{\partial}{\partial y}\left(\Phi\frac{\partial\Phi}{\partial y}\right)\right\}\mathrm{d}x\mathrm{d}y = \int\limits_{C}\left(-\Phi\frac{\partial\Phi}{\partial y}\mathrm{d}x + \Phi\frac{\partial\Phi}{\partial x}\mathrm{d}y\right). \tag{A 3}$$

Here C is a positively (counterclockwise) oriented contour along the boundary of the periodic domain occupied by fluid shown in Figure 9. A sum of integrals along left and right hand sides (vertical segments) of the contour vanishes due to periodicity. Integral along lower part of the contour (horizontal segment) is zero due to the boundary condition on potential $\Phi_{y=-\infty} = 0$. Notice that in the case of finite depth fluid with a rigid flat

bottom $y=-h$, the integral along similar lower segment $y=-h$ is also zero because the boundary condition at the finite depth bottom is $\Phi_y|_{y=-h}=0$ (zero vertical velocity at the bottom) and $\mathrm{d}y=0$. Then the equation (A 3) is reduced to the following line integral

$$2T=\int\limits_{x=\lambda/2,\ y=\eta(x,t)}^{x=-\lambda/2}\left(-\Phi\frac{\partial\Phi}{\partial y}\mathrm{d}x+\Phi\frac{\partial\Phi}{\partial x}\mathrm{d}y\right). \tag{A 4}$$

We use the time-dependent conformal transformation (2.6),(2.7) to relate partial derivatives in x,y and u,v as follows

$$\frac{\partial\Phi}{\partial u}=\frac{\partial\Phi}{\partial x}x_u+\frac{\partial\Phi}{\partial y}y_u,$$
$$\frac{\partial\Phi}{\partial v}=\frac{\partial\Phi}{\partial x}x_v+\frac{\partial\Phi}{\partial y}y_v,$$

which implies that

$$\frac{\partial\Phi}{\partial x}=\frac{\Phi_u x_u-\Phi_v y_u}{x_u^2+y_u^2}, \tag{A 5}$$
$$\frac{\partial\Phi}{\partial y}=\frac{\Phi_u y_u+\Phi_v x_u}{x_u^2+y_u^2}, \tag{A 6}$$

where we also used Cauchy-Riemann equations $x_u=y_v$ and $x_v=-y_u$ for the conformal map $z(w)$.

Substituting (A 5) and (A 6) into (A 4), using relations $\mathrm{d}x=x_u\mathrm{d}u$ and $\mathrm{d}y=y_u\mathrm{d}u$ on the line $w=u$ one obtains that

$$2T=\int\limits_{\lambda/2}^{-\lambda/2}\left(-\Phi_v\Phi\right)|_{v=0}\,\mathrm{d}u=\int\limits_{-\lambda/2}^{\lambda/2}\Phi_v\Phi|_{v=0}\,\mathrm{d}u. \tag{A 7}$$

Here we took into account the orientation of the contour and conditions (2.7) on conformal transformation.

Sokhotski-Plemelj theorem (5.1) (see e.g. Gakhov (1966); Polyanin & Manzhirov (2008)) allows to express a real part of the function which is analytic in the lower (upper) half plane through the imaginary part (and vice versa) at the real line $u=w$ using the Hilbert transformation (2.12). For a conformal transformation $z(w,t)=x(w,t)+\mathrm{i}y(w,t)$ such relations are given by (2.29). A complex velocity potential $\Pi(z,t)=\Phi+\mathrm{i}\Theta$ is the analytic function in the fluid domain $-\infty<y\leqslant\eta(x,t)$, where Θ is the stream function. The conformal transformation $z=z(w,t)$ (2.6) ensures that Π remains analytic function after transforming from z to w variable with the lower half plane $\mathbb{C}^-$ being the domain of analyticity in w. Similar to equation (2.29), real and imaginary parts of Π are related at the real line $u=w$ through the Hilbert transformation as follows

$$\Theta=\hat{H}\Phi,\quad \Phi=-\hat{H}\Theta, \tag{A 8}$$

where we assumed the decaying boundary condition $\Phi|_{v=-\infty}=\Theta|_{v=-\infty}=0$. Here we abuse notation and use the same Π and Φ both for independent variables w and z : $\tilde{\Phi}(w,t)\equiv\Phi(z,t)$ and $\tilde{\Pi}(w,t)\equiv\Pi(z,t)$, i.e. we omit tilde.

Also the analyticity of Π implies that the velocity potential Φ is the harmonic function satisfying the Laplace equation (2.1) both in x,y variables and similarly

$$\nabla^2\Phi(u,v,t)=0$$

in variables u and v. Using Cauchy-Riemann equations (2.15) and the relations (A 8) one obtains that

$$\Phi_v = -\hat{H}\Phi_u. \tag{A 9}$$

Substituting (A 9) into (A 7) we express the kinetic energy in terms of canonical variable ψ as follows

$$2T = \int\limits_{-\lambda/2}^{\lambda/2} \Phi_v \Phi|_{v=0}\, \mathrm{d}u = -\int\limits_{-\lambda/2}^{\lambda/2} \psi \hat{H} \psi_u \mathrm{d}u, \tag{A 10}$$

Here we used the definition (2.5) which in w plane turns into $\psi(u,t) \equiv \Phi(u, v=0, t)$ as follows from the mapping of the fluid surface into the real line $v = 0$. Then the Hamiltonian in terms of variables on the surface takes the following form

$$H = -\frac{1}{2}\int\limits_{-\lambda/2}^{\lambda/2} \psi \hat{H} \psi_u \mathrm{d}u + \frac{g}{2}\int\limits_{-\lambda/2}^{\lambda/2} y^2 x_u \mathrm{d}u. \tag{A 11}$$

A.2. *Least action principle in conformal variables*

We use the constrained Lagrangian formulation to obtain the dynamical equations in conformal variables at fluid surface. A time dependence of the map (2.6) implies that we have to ensure the analyticity of that map through the appropriate constraint. We discuss the Lagrangian dynamics first and add the corresponding constraint later in this Section. Equations (A 1) realize extremum of an action

$$S = \int\limits_{t_1}^{t_2} L \mathrm{d}t, \tag{A 12}$$

with the Lagrangian

$$L = \int\limits_{-\lambda/2}^{\lambda/2} \psi \frac{\partial \eta}{\partial t} \mathrm{d}x - H. \tag{A 13}$$

The first term here has to be converted from the integral over x into u variable. Consider mapping $(x,t) \to (u,\tau)$, which is the change of parametrization of the surface under the conformal map. Here $\tau = t$. Transformation $u = u(x,t)$ is the inverse to the conformal map $x = x(u,\tau)$. The fluid surface $\eta(x,t)$ after transformation corresponds to $y(u,\tau)$. We express $\partial\eta/\partial t$ by the chain rule as follows

$$\frac{\partial \eta}{\partial t} = \frac{\partial y}{\partial \tau}\frac{\partial \tau}{\partial t} + \frac{\partial y}{\partial u}\frac{\partial u}{\partial t} = \frac{\partial y}{\partial \tau} + \frac{\partial y}{\partial u}\frac{\partial u}{\partial t}. \tag{A 14}$$

To find $\partial u/\partial t$ here we express full differentials of x and t through u and τ as follows

$$\begin{pmatrix} \mathrm{d}x \\ \mathrm{d}t \end{pmatrix} = \begin{pmatrix} x_u & x_\tau \\ t_u & t_\tau \end{pmatrix} \begin{pmatrix} \mathrm{d}u \\ \mathrm{d}\tau \end{pmatrix} \equiv J \begin{pmatrix} \mathrm{d}u \\ \mathrm{d}\tau \end{pmatrix}. \tag{A 15}$$

Taking into account that $\tau = t$, one obtains the Jacobian matrix

$$J = \begin{pmatrix} x_u & x_\tau \\ 0 & 1 \end{pmatrix}. \tag{A 16}$$

Inverse procedure for full differentials of u and τ through x and t yields that

$$\begin{pmatrix} \mathrm{d}u \\ \mathrm{d}\tau \end{pmatrix} = \begin{pmatrix} \partial u/\partial x & \partial u/\partial t \\ \partial \tau/\partial x & \partial \tau/\partial t \end{pmatrix} \begin{pmatrix} \mathrm{d}x \\ \mathrm{d}t \end{pmatrix} = J^{-1} \begin{pmatrix} \mathrm{d}x \\ \mathrm{d}t \end{pmatrix}. \tag{A 17}$$

Comparing entries of the matrix in (A 17) with inverse of (A 16), one gets

$$\frac{\partial u}{\partial t} = -\frac{x_\tau}{x_u}. \tag{A 18}$$

Substituting (A 18) into (A 14) yields

$$\frac{\partial \eta}{\partial t} = y_\tau - y_u \frac{x_\tau}{x_u}. \tag{A 19}$$

We use the Lagrangian (A 13) to substitute it into the action (A 12). Consider the first term in the action,

$$S = \int\int L\mathrm{d}t = \int\int \psi \frac{\partial \eta}{\partial t} \mathrm{d}x\mathrm{d}t + \dots \tag{A 20}$$

and perform a change of variables in the integral as $\mathrm{d}x\mathrm{d}t = \det(J)\mathrm{d}u\mathrm{d}\tau = x_u \mathrm{d}u\mathrm{d}\tau$. Together with the expression (A 19) it results in

$$\int\int \psi \frac{\partial \eta}{\partial t} \mathrm{d}x\mathrm{d}t = \int\int \psi \left(y_\tau - y_u \frac{x_\tau}{x_u} \right) x_u \mathrm{d}u\mathrm{d}\tau = \int\int \psi (y_\tau x_u - y_u x_\tau) \mathrm{d}u\mathrm{d}\tau. \tag{A 21}$$

Using (A 11), (A 13), (A 21) and adding the analyticity constraint (2.29) ensuring that $\tilde{y} - y_0 = \hat{H}\tilde{x}$ and taking into account that $\tau = t$ as well we obtain a new constrained Lagrangian

$$L = \int_{-\lambda/2}^{\lambda/2} \psi (y_t x_u - y_u x_t) \mathrm{d}u + \frac{1}{2} \int_{-\lambda/2}^{\lambda/2} \psi \hat{H} \psi_u \mathrm{d}u - \frac{g}{2} \int_{-\lambda/2}^{\lambda/2} y^2 x_u \mathrm{d}u + \int_{-\lambda/2}^{\lambda/2} (y - \tilde{y}_0 - \hat{H}\tilde{x}) f \mathrm{d}u, \tag{A 22}$$

where f is the Lagrange multiplier for the analyticity constraint.

A.3. *Variations of action*

We now obtain the dynamical equations from the Hamilton's least action principle. Vanishing of variational derivative $\delta S/\delta\psi = 0$ of the action (A 12) with the Lagrangian (A 22) over potential ψ on the surface yields the following expression

$$y_t x_u - y_u x_t + \hat{H}\psi_u = 0. \tag{A 23}$$

This equation is nothing else but kinematic boundary condition (2.2) after the conformal map into w plane.

Two conditions $\delta S/\delta x = 0$ and $\delta S/\delta y = 0$ result in equations

$$y_u \psi_t - y_t \psi_u + g y y_u = \hat{H} f, \tag{A 24}$$

$$-x_u \psi_t + x_t \psi_u - g y x_u = f, \tag{A 25}$$

which are turned into a single equation by excluding the Lagrange multiplier f giving

$$y_u \psi_t - y_t \psi_u + \hat{H}(x_u \psi_t - x_t \psi_u) + g[y y_u + \hat{H}(y x_u)] = 0. \tag{A 26}$$

Equations (A 23) and (A 26) recover the implicit dynamical equations (2.10) and (2.11).

A.4. *Zeroth harmonic in implicit dynamical equations* (2.10) *and* (2.11) *and conservation of momentum*

Consider Fourier transformations of the surface elevation $y(u,t)$ and the velocity potential on surface ψ with respect to conformal coordinate u,

$$\begin{aligned} y(u,t) &= y_0(t) + \sum_{k\neq 0} y_k(t) \mathrm{e}^{\mathrm{i}ku}, \\ \psi(u,t) &= \psi_0(t) + \sum_{k\neq 0} \psi_k(t) \mathrm{e}^{\mathrm{i}ku}. \end{aligned} \tag{A 27}$$

Here zeroth harmonics $y_0(t)$ and $\psi_0(t)$ are written separately and are given by

$$y_0(t) = \frac{1}{\lambda} \int\limits_{-\lambda/2}^{\lambda/2} y(u,t)\mathrm{d}u, \quad \psi_0(t) = \frac{1}{\lambda} \int\limits_{-\lambda/2}^{\lambda/2} \psi(u,t)\mathrm{d}u. \tag{A 28}$$

One can rewrite equation (A 26) in the following form

$$y_u\psi_t - y_t\psi_u = -\hat{H}(x_u\psi_t - x_t\psi_u + yx_u) - \frac{g}{2}\frac{\partial}{\partial u}y^2. \tag{A 29}$$

A zeroth Fourier harmonic of the right hand side (r.h.s.) of equation (A 29) vanishes because the term in parenthesis is multiplied by $\hat{H}$ which removes any zeroth harmonic and the remaining term is the partial derivative over u. Respectively, the zeroth harmonic of the left hand side (l.h.s.) of equation (A 29) must vanish. Integrating that l.h.s. to obtain the zeroth harmonic, using equation (A 29) and integrating by parts over u one obtains that

$$\frac{1}{\lambda} \int\limits_{-\lambda/2}^{\lambda/2} (y_u\psi_t - y_t\psi_u)\mathrm{d}u = \frac{1}{\lambda} \int\limits_{-\lambda/2}^{\lambda/2} (y_u\psi_t + y_{ut}\psi)\mathrm{d}u = \frac{1}{\lambda}\frac{\partial}{\partial t} \int\limits_{-\lambda/2}^{\lambda/2} \psi y_u \mathrm{d}u = 0, \tag{A 30}$$

where we used a periodicity of ψ and y in u. Thus $\int\limits_{-\lambda/2}^{\lambda/2} \psi y_u \mathrm{d}u$ is the integral of motion. To find a physical meaning of that integral we note that natural candidates for conserved quantities are the components of the total momentum of fluid along x and y directions. Taking into account that fluid density is one, we obtain x component of momentum P_x as an integral of the horizontal velocity inside fluid, which gives

$$P_x = \int\limits_{-\lambda/2}^{\lambda/2} \mathrm{d}x \int\limits_{-\infty}^{\eta(x,t)} \Phi_x \mathrm{d}y = \int\limits_C \Phi \mathrm{d}y = \int\limits_{\lambda/2}^{-\lambda/2} \Phi \left.\frac{\partial y}{\partial x}\right|_{y=\eta(x,t)} \mathrm{d}x = -\int\limits_{-\lambda/2}^{\lambda/2} \psi y_u \mathrm{d}u. \tag{A 31}$$

Here we applied Green's theorem to positively oriented contour C shown in Figure 9. Due to periodicity of functions and decaying boundary condition $\Phi(x,y,t)|_{y\to-\infty} = 0$, only integral along the surface is nonzero. Comparison of equations (A 30) and (A 31) shows that consistency of equation (A 29) is ensured by the conservation of the horizontal component P_x of the total momentum of the fluid.

Applying the Hilbert transformation $\hat{H}$ to equation (A 29) and using the identity (2.28) one obtains that

$$x_u\psi_t - x_t\psi_u + yx_u - q_0 = \hat{H}\left(y_u\psi_t - y_t\psi_u + \frac{g}{2}\frac{\partial}{\partial u}y^2\right), \tag{A 32}$$

where q_0 is the zeroth Fourier harmonic of $x_u\psi_t - x_t\psi_u + yx_u$. To find q_0 we proceed

similar to equations (A 30) and (A 31) to find that

$$q_0 = \frac{1}{\lambda}\int\limits_{-\lambda/2}^{\lambda/2}(x_u\psi_t - x_t\psi_u + yx_u)\mathrm{d}u = \frac{1}{\lambda}\frac{\partial}{\partial t}\int\limits_{-\lambda/2}^{\lambda/2}\psi x_u\mathrm{d}u + \frac{1}{\lambda}\int\limits_{-\lambda/2}^{\lambda/2} yx_u\mathrm{d}u, \tag{A 33}$$

where $\int\limits_{-\lambda/2}^{\lambda/2}\psi x_u\mathrm{d}u$ is the integral of motion corresponding to the conservation of the vertical component P_y of the total momentum of fluid,

$$P_y = \int\limits_{-\lambda/2}^{\lambda/2}\mathrm{d}x\int\limits_{-\infty}^{\eta(x,t)}\Phi_y\mathrm{d}y = \int\limits_C -\Phi\mathrm{d}x = \int\limits_{-\lambda/2}^{\lambda/2}\psi x_u\mathrm{d}u. \tag{A 34}$$

Then equations (A 33) and (A 34) imply that q_0 is the integral of motion given by

$$q_0 = \frac{1}{\lambda}\int\limits_{-\lambda/2}^{\lambda/2} yx_u\mathrm{d}u = \frac{1}{\lambda}\int\limits_{-\lambda/2}^{\lambda/2}\eta(x,t)\mathrm{d}x \tag{A 35}$$

and representing a conservation of the total mass of fluid. Also according to equation (2.17), we set $q_0 = 0$ in this paper.

Appendix B. Alpert-Greengard-Hagstrom (AGH) Algorithm and Stokes Wave

In this Appendix we describe an efficient algorithm for Padé approximation of the function on a discrete grid, following original work Alpert *et al.* (2000) and work by Lau (2004) where more detailed explanation and further development of the algorithm was presented.

Consider 2π-periodic complex-valued function $f(u) = z(u) - u - \mathrm{i}y_0$ defined on a grid with nodes $u_j \in [-\pi, \pi]$. Values of the function at the grid points are denoted as $f_j = f(u_j)$. We look for an approximation of $f(u)$ in the form of a ratio of two polynomials $P(u)$ and $Q(u)$, i.e. the Padé approximation. We briefly describe AGH algorithm in a general way with additional comments for our particular case. As it was mentioned in Section 4, we use the second conformal map $\zeta = \tan(u/2)$. The introduction of auxiliary variable ζ allows to consider the real line $\zeta \in \mathbb{R}$ as opposed to considering a finite interval $u \in [-\pi, \pi]$, while the infinity along the imaginary axis is mapped into imaginary unit i and 2π-periodicity in u direction is ensured. Without loss of generality we assume that $f(\pm\pi) = 0$. In this paper, we take $f(u) = z(u) - u - \mathrm{i}y_0 = \tilde{z}(u) - \mathrm{i}y_0$ (see equations (4.5) and (4.6) for comparison). Condition $f(\pm\pi) = 0$ allows to consider P and Q such that the degree of polynomials are $\deg Q = 1 + \deg P = N$, where the integer N is allowed to vary. We are looking for the convergence of the rational approximation to f,

$$\frac{P(\zeta)}{Q(\zeta)} \to f(\zeta),$$

in a sense of solving a minimization problem

$$\min_{P,Q}\int\limits_{-\pi}^{+\pi}\left|\frac{P(u)}{Q(u)} - f(u)\right|^2\mathrm{d}u. \tag{B 1}$$

That minimization problem is challenging because Q in the denominator makes (B 1) nonlinear problem. In the transformed variable ζ the problem (B 1) remains nonlinear and is reduced to

$$\min_{P,Q} \int_{-\infty}^{+\infty} \left| \frac{P(\zeta)}{Q(\zeta)} - f(\zeta) \right|^2 \frac{\mathrm{d}\,\zeta}{\zeta^2+1}. \tag{B 2}$$

In AGH algorithm, the complexity of nonlinearity is bypassed by solving instead of (B 1), a sequence of linear least-square problems

$$\min_{P^{(i+1)},Q^{(i+1)}} \int_{-\infty}^{+\infty} \left| \frac{P^{(i+1)}(u)}{Q^{(i)}(u)} - \frac{Q^{(i+1)}(u)}{Q^{(i)}(u)} f(u) \right|^2 \mathrm{d}u, \;\; i = 1, 2, \ldots \tag{B 3}$$

We define an inner product

$$\langle f, g \rangle_i = \int_{-\infty}^{+\infty} f(u) \bar{g}(u) w_i(u) \mathrm{d}u, \tag{B 4}$$

with a weight function $w_i(u) = \frac{1}{|Q^{(i)}(u)|^2}$ (for ζ-plane the formula for the weight is modified to be $w_i(\zeta) = 1/(|Q^{(i)}(\zeta)|^2(\zeta^2+1))$). Then the previous least squares problem can be rewritten as follows

$$\min_{P^{(i+1)},Q^{(i+1)}} || - P^{(i+1)}(u) + Q^{(i+1)}(u) f(u) ||_i, \tag{B 5}$$

where

$$||g(u)||_i^2 = \langle g, g \rangle_i$$

is the norm.

As it was shown in Alpert *et al.* (2000), the solution of the least squares problem (B 5) is equivalent to the solution of

$$\langle -P^{i+1} + Q^{i+1} f(u), h_n(u) \rangle_i = 0,$$

for $n = 1, \ldots, 2N$, with $h_n(u)$ defined as follows

$$\begin{cases} u^{n/2-1}, & \text{for } n = 2, 4, 6, \ldots, 2N, \\ u^{(n-1)/2} f(u), & \text{for } n = 1, 3, 5, \ldots, 2N-1, \end{cases} \tag{B 6}$$

which are nothing else but

$$f(u), 1, uf(u), u, u^2 f(u), \ldots, u^{N-1} f(u), u^{N-1}, u^N f(u).$$

This claim can be proven by variation of mth coefficient of $P(u)$ (for even $n = 2m+2$) and $Q(u)$ (for odd $n = 2m+1$). We put coefficient at the leading power of $Q(u)$ to be equal to one. Thus we need to find $2N$ coefficients for two polynomials.

We orthogonalize $2N+1$ functions $h_n(u)$ using Gramm-Schmidt orthogonalization procedure,

$$g_n(u) = \begin{cases} f(u), & \text{for } n = 1, \\ 1 - c_{21} f(u), & \text{for } n = 2, \\ u g_{n-2}(u) - \sum\limits_{j=1}^{\min\{4,n-1\}} c_{nj} g_{n-j}(u), & \text{for } n = 3, \ldots, 2N+1, \end{cases} \tag{B 7}$$

where real constants c_{nj} are given by

$$c_{nj} = \begin{cases} \frac{\langle 1, f(u)\rangle_i}{\langle f(u), f(u)\rangle_i}, & \text{for } n = 2 \text{ and } j = 1, \\ \frac{\langle (ug_{n-2}, g_{n-j}\rangle_i}{\langle g_{n-j}, g_{n-j}\rangle_i}, & \text{for } n = 3, \ldots, 2N+1 \text{ and } j = 1, \ldots, \min\{4, n-1\}. \end{cases} \tag{B 8}$$

Then we obtain that

$$g_{2N+1} = -P^{(i+1)} + f(u)Q^{(i+1)}, \tag{B 9}$$

so $P^{(i+1)}$ and $Q^{(i+1)}$ are computed from recurrence coefficients c_{nj} by splitting into even and odd-numbered parts.

For our purposes of finding the jump at branch cut it is convenient to represent a ratio of $P(u)$ and $Q(u)$ as a sum of simple poles,

$$\frac{P(u)}{Q(u)} = \sum_{n=1}^{N} \frac{\gamma_n}{u - \chi_n}. \tag{B 10}$$

In order to do that we compute zeros χ_n, $n = 1, 2, \ldots, N$ of $Q(u)$ using Newton's iterations. At each step one zero χ_n is found by Newton's iterations. After that we remove that zero from $Q(u)$ by division on $(u - \chi_n)$ and proceed to the next step for the modified Q etc. After that procedure coefficients γ_n are given by the following expression

$$\gamma_n = \frac{P(\chi_n)}{Q'(\chi_n)}. \tag{B 11}$$

Derivative $Q'(u)$ are obtained from previous recurrence relation for $g_n(u)$ by differentiation.

Appendix C. Tables of Stokes Waves

Using the Padé approximation, introduced in Section 4, one can approximate Stokes wave for each value of the scaled height H/λ as a sum of poles

$$z(w) \simeq z_{pade}(u) \equiv w + \mathrm{i}y_0 + \sum_{n=1}^{N} \frac{\gamma_n}{\tan(w/2) - \mathrm{i}\chi_n}. \tag{C 1}$$

Here N is the number of poles in the Padé approximation. Using AGH algorithm (see Appendix B) we found that all poles for all values of H/λ are located on the imaginary axis.

We provide Tables 1-4 for four particular cases of Stokes waves with wave heights ranging from $H/L \simeq 0.031791$ to $H/L \simeq 0.141058$. Complete library of computed waves can be accessed through the electronic attachments as well as through the web link Dyachenko *et al.* (2015). These data of Padé approximation allow to recover the Stokes wave with the relative accuracy of at least 10^{-26} (for the vast majority of cases the actual accuracy is higher by several orders of magnitude). First and second columns of both Tables and electronic files represent values of χ_n and γ_n, respectively. Additionally a third column in electronic files provides the values of $\rho_{n,N}$, $n = 1, 2, \ldots, N$ calculated from data of the first two columns using equations (4.8*a*), (4.11) and (4.12).

We used three quantities to characterize the accuracy of our numerical Stokes wave solution and its Padé approximation. First quantity is the residue

$$R(y) \equiv N^{-1/2} \left(\sum_{j=1}^{M} |\hat{L}_0 y(u_j)|^2 \right)^{1/2}$$

of equation (2.33). $R(y)$ characterizes convergence of our iteration algorithm described in Section 3.1 to the Stokes wave. Here $M = 2k_{max}$ is the number of grid points u_j used in the discretization of $z(u)$. Second quantity is the relative error of Padé approximation

$$err_{pade} = \left(\frac{\sum_{j=1}^{M} |z(u_j) - z_{pade}(u_j)|^2}{\sum_{j=1}^{M} |z(u_j)|^2} \right)^{1/2}$$

of our numerical solution $z(u_j)$. Third quantity is the amplitude of the highest Fourier harmonics $|\hat{z}_{k_{max}}|$ used in FFT.

We balanced these three quantities in our simulation to achieve the most efficient and reliable approximants of Stokes waves. Typically we chose k_{max} large enough such that $|\hat{z}_{k_{max}}| < M^{-1/2}10^{-26}$ to ensure that our discretization error is below 10^{-26}. Here the factor $M^{-1/2}$ characterize the accumulation of round-off error in FFTs. A convergence of numerical iterations down to $R(y) \simeq 10^{-28}$ was found to be sufficient to achieve the desired accuracy of solution in 10^{-26}. After that we used AGH algorithm with N large enough to make sure that err_{pade} is below 10^{-26} by several orders of magnitude.

The second and third rows in electronic `.dat`-files provide the additional information extracted from simulations which include the number of points of the numerical grid $M = 2k_{max}$, the residual $R(y)$, the Stokes wave height y_0 at $x = \pm\pi$, the amplitude of the highest Fourier harmonics $|\hat{z}_{k_{max}}|$, the Padé error err_{pade}, the scaled Stokes wave height H/λ and the Stokes wave velocity c. Values of H/λ are also encoded in the names of `.dat`-files. Also the file `summary.txt` provides a summary of the results from all `.dat`-files.

k	χ_k	γ_k
1	9.960410926063350838629927461086 61e-01	7.869552677988157798969409753847 30e-03
2	9.789729250875445172888517550054 98e-01	1.589382086499895499702201560075 58e-02
3	9.495696039189825344346113276595 88e-01	2.092704779146660674627624449578 13e-02
4	9.104061186787678010118840229983 71e-01	2.307728553092327749219270329785 93e-02
5	8.646947688440237758493182926327 06e-01	2.278218233955356162992824674540 14e-02
6	8.157843926449677882643709022390 31e-01	2.067815693342508983225820736170 42e-02
7	7.667745188044647471112111332869 36e-01	1.745050182918683906672019765498 62e-02
8	7.202839012067852205952814179790 68e-01	1.371915186205552703870528555878 68e-02
9	6.783654204131271307510571417053 42e-01	9.979034893934588248110470184706 10e-03
10	6.425274847908419676615854772314 96e-01	6.587399446001104384033942670242 05e-03
11	6.138146677650695620129857020142 92e-01	3.780226209360030420363906187924 91e-03
12	5.929083157742315710201020784180 28e-01	1.700684389166557586805616649692 51e-03
13	5.802208826392953721044026130453 57e-01	4.279395361919985118980051772408 95e-04

TABLE 1. Data for Padé approximation of the wave with velocity $c = 1.005$, the steepness $H/\lambda = 0.031791185830078550217424174610939$, and $y_0 = -0.094819818875344225940453182945545$. Parameters of simulations and Padé approximation are $M = 16384$, $R(y) \simeq 3.64 \times 10^{-33}$, $err_{pade} \simeq 4.65 \times 10^{-31}$, and the smallest Fourier harmonic had value $|\hat{z}_{k_{max}}| \simeq 1.00 \times 10^{-39}$.

k	χ_k	γ_k
1	9.95104877443162988543285604210300e-01	9.86344259137750131929660816853428e-03
2	9.74036453796113160099814623502153e-01	2.04507668432927246329100238980833e-02
3	9.37570348097817646693771937993553e-01	2.79392155141519735983551710052556e-02
4	8.88487837568099082583936075213862e-01	3.23466950514503536891484865775305e-02
5	8.30226745019764721513358604279726e-01	3.40147781594254640293216855633111e-02
6	7.66333992991599455804305516283483e-01	3.35031653839781443242921103012960e-02
7	7.00044654389407424698796692053902e-01	3.14489535896823273634285653396772e-02
8	6.34030062620564487061621925382604e-01	2.84500818501058994363745193170182e-02
9	5.70306175038391450182479612388228e-01	2.49972283728050063777939045774063e-02
10	5.10259067527902434999804572718914e-01	2.14511658748252720344184761694938e-02
11	4.54736803912594713785686635920502e-01	1.80506679368664453110659093724408e-02
12	4.04166063099136862080187337641328e-01	1.49353242488736140402002871952586e-02
13	3.58666596761459474167122202709l0e-01	1.21719831322217078183473222652247e-02
14	3.18149576080072883402812844826148e-01	9.77859794087821305028150640251530e-03
15	2.82395821449537219671027831006306e-01	7.74304960914297497673324174361282e-03
16	2.51113624911206124013006119628666e-01	6.03673166180751660604462350895498e-03
17	2.23980136883660703565243361779229e-01	4.62368871094252860720889700284368e-03
18	2.00669410169964201214033391681290e-01	3.46637996984113299044046402602488e-03
19	1.80870715726851513117763940777923e-01	2.52906751261377992038440816275726e-03
20	1.64299946133899344356900387886524e-01	1.77962987225519971005973434397249e-03
21	1.50706307186061197360270221491920e-01	1.19038860012342014795358493343618e-03
22	1.39875923302152112463866847539994e-01	7.38354660230910637368329193600582e-04
23	1.31633517886184493678824771993353e-01	4.05164363997062298811235878087573e-04
24	1.25842975665215746611096122396649e-01	1.76877312168739070195683856144061e-04
25	1.22407333541749966033626434463374e-01	4.37430353029634816661994533800963e-05

TABLE 2. Data for Padé approximation of the wave with velocity $c = 1.051$, the steepness $H/\lambda = 0.10042675172528485854673515635249$, and $y_0 = -0.25732914098527682158156915646871$. Parameters of simulations and Padé approximation are $M = 16384$, $R(y) \simeq 5.19 \times 10^{-32}$, $err_{pade} \simeq 1.69 \times 10^{-31}$, and the smallest Fourier harmonic had value $|\hat{z}_{k_{max}}| \simeq 1.00 \times 10^{-37}$.

k	χ_k	γ_k
1	9.954338259326085501323840348572l3e-01	9.065139686595942639941549838590 22e-03
2	9.757207327298723616616390754455 56e-01	1.881041724798676256079883776650 13e-02
3	9.414585806990367969839897495006 3e-01	2.580242682400627707377450511100 2e-02
4	8.950720791981099348658101255969 55e-01	3.007603153027648717903697068337 79e-02
5	8.396033688600360062788108209839 49e-01	3.191678517911005432446988074890 31e-02
6	7.782467078461258645302697380953 48e-01	3.179007767615355293105958799648 77e-02
7	7.139774635954800039119191533274 80e-01	3.023354673070953858782308779159 97e-02
8	6.493143751272693580257907239638 70e-01	2.776253841587461060851492287734 01e-02
9	5.862154659289895769511203662455 81e-01	2.481078428845997070485208159112 64e-02
10	5.260779374477518729842757281015 22e-01	2.170683511443522377601783718530 73e-02
11	4.698024074039504859655040299969 14e-01	1.867629415251176997453766702895 00e-02
12	4.178862693761100400458688195922 73e-01	1.585799691440043491249612582542 60e-02
13	3.705214441823407638844200276668 27e-01	1.332485107367400595858129921622 63e-02
14	3.276824397559602135104673636060 42e-01	1.110372838809772327817086869350 09e-02
15	2.891987225491722396077215843436 98e-01	9.191852851050633186230966178611 30e-03
16	2.548104663546661958166653706869 97e-01	7.569078251493162246283659744106 75e-03
17	2.242093673347215895745330374663 43e-01	6.206445341954405924238468203094 5e-03
18	1.970672250670653975412469301064 41e-01	5.071771623152349896739901189196 96e-03
19	1.730550913622684511203640813346 65e-01	4.133079628544919675547780577629 08e-03
20	1.518554620265324361041493613792 10e-01	3.360507861676747839977998260835 50e-03
21	1.331695155402037881566421669065 91e-01	2.727248943163220723252772218444 58e-03
22	1.167209332747012910000887725539 493e-01	2.209868559536908864195883677066 23e-03
23	1.022574314059190381782750317362 90e-01	1.788263902643219993982797711282 06e-03
24	8.955081272838585941164070196018 20e-02	1.445426573285507268570802527496 22e-03
25	7.839610283199306147671730880202 79e-02	1.167114421958040195586651265394 27e-03
26	6.861015668544666162109765392891 58e-02	9.414954328941759378428749274212 05e-04
27	6.002999411849052707026523249821 35e-02	7.587997371527525498545921476659 95e-04
28	5.251103313869987008182479745092 58e-02	6.109986993623727839976913909664 87e-04
29	4.592532812312476670073655998679 43e-02	4.915194832982088179830412333839 80e-04
30	4.015987779685882671959199959477 10e-02	3.949972697727407591207473014934 0e-04
31	3.511503969883829009722288745251 09e-02	3.170638153025694372427807688384 13e-04
32	3.070306930716330258560683264246 87e-02	2.541692636551890662419874345561 00e-04
33	2.684679013238119523211856180745 78e-02	2.034333800263327731865916723375 83e-04
34	2.347839373167086812886400256351 46e-02	1.625222377073820770963023548225 32e-04
35	2.053836421786788398200647846559 08e-02	1.295465762646297880752764528263 28e-04
36	1.797451938526141177771030840102 65e-02	1.029783990186871481728858681966 23e-04
37	1.574115937048060903319199979284 06e-02	8.158278627638570842357761035944 81e-05
38	1.379831338394457508068597362035 07e-02	6.436231473510347582817735729952 89e-05
39	1.211107520130283581880071919350 72e-02	5.051186462827321660855071341511 95e-05
40	1.064901859107799229665305598240 50e-02	3.938195073259443591842981125136 36e-05
41	9.385684526520129564020753692902 78e-03	3.044902563491799132507245769560 79e-05
42	8.298132784394209253513548810963 43e-03	2.329147305448851871076048073040 53e-05
43	7.366551303394894387451775662373 21e-03	1.757023795308984361814173578063 91e-05
44	6.573917418137901892835109163050 43e-03	1.301323253617935853123055629509 35e-05
45	5.905705780804604148025239131594 00e-03	9.402817559811809735105347269285 33e-06
46	5.349638427594850462834968387777 43e-03	6.565791308229329543809441144410 17e-06
47	4.895473045077889708041442627293 96e-03	4.365428708997594713227716538314 21e-06
48	4.534826046882471344856907837631 08e-03	2.695204314458018483141296860519 70e-06
49	4.261027587864338928412732759054 55e-03	1.473908712155928194371709433881 63e-06
50	4.069006126790112630317774027889 05e-03	6.419312711264881056574661765998 01e-07
51	3.955200608617434124106504749940 64e-03	1.585355986424909079422305325114 50e-07

TABLE 3. Data for Padé approximation of the wave with velocity $c = 1.0929$, the steepness $H/\lambda = 0.13825830866311310404416736817381$, and $y_0 = -0.29153391724312882929999650320 09$. Parameters of simulations and Padé approximation are $M = 65536$, $R(y) \simeq 2.59 \times 10^{-31}$, $err_{pade} \simeq 1.01 \times 10^{-32}$, and the smallest Fourier harmonic had value $|\hat{z}_{k_{max}}| \simeq 5.00 \times 10^{-38}$.

k	χ_k	γ_k
1	9.93398643583003025153415435504531e-01	1.28741415762741679346145664996829e-02
2	9.65060482058669453480870980252106e-01	2.60267721567181859054226183119919e-02
3	9.16714789789161849202896809849705e-01	3.43697679627825352269776411757291e-02
4	8.53133231672953078297597841861823e-01	3.81940153445550033591099941584920e-02
5	7.79861194757267505357891461462460e-01	3.83579555843352602595202964927154e-02
6	7.02176870736814955937036169062899e-01	3.59774931820106663192752740784546e-02
7	6.24431910013545641111933110534714e-01	3.21282856711997437340001627375168e-02
8	5.49795332847499273525022520666518e-01	2.76691730121067711930378384900232e-02
9	4.80296232546974823630387324524545e-01	2.31906560517515347893552651709825e-02
10	4.17024645857800791824977075950470e-01	1.90429324287558759377242844714520e-02
11	3.60378305224974615221811203424356e-01	1.53959152585563261217878597243142e-02
12	3.10289842646985418345605736936048e-01	1.23006351687210032636876990145911e-02
13	2.66407648266938619328412589947 21e-01	9.73852232172353639036354649203610e-03
14	2.28226886286517332438415939592608e-01	7.65583101348162009153247587551195e-03
15	1.95177843545134733789119725180096e-01	5.98535170044127311114464478095979e-03
16	1.66681805023593130823224346797399e-01	4.65887488461708640776107914945203e-03
17	1.42183993584453030868317439497003e-01	3.61357577121517253016005783742974e-03
18	1.21171172484979583446779037786714e-01	2.79470260489814969664959294926652e-03
19	1.03179452511723992079582272565214e-01	2.15617836676118577227243251241331e-03
20	8.77961228595568606401648108610398e-02	1.66012679310648786275121618740345e-03
21	7.46580315447597465030574978595406e-02	1.27592107645668605269203574613739e-03
22	6.34481306443940719507463127666211e-02	9.79089087450639485345366472519338e-04
23	5.38911872290903942028496746096495e-02	7.50248095624531518737269429111365e-04
24	4.57492587887819300483008251206986e-02	5.74148509163471182463355721181721e-04
25	3.88172752742240105088258746631741e-02	4.38854383779301056123215099079188e-04
26	3.29189096590597195144947958198357e-02	3.35061475940689863018834966768472e-04
27	2.79028212558501660025568098114343e-02	2.55540871176311150876065830758264e-04
28	2.36392981742008042750164949870111e-02	1.94691329540109355414952726522057e-04
29	2.00172924085211268884110103807234e-02	1.48182722053010736525844218770677e-04
30	1.69418235041002160106748854919734e-02	1.12674155188771601572543993641392e-04
31	1.43317184931477833930656499987995e-02	8.55924207962470484084537963575900e-05
32	1.21176530092033068365142201489852e-02	6.49586463790799447674548874436684e-05
33	1.02404588173178159766150762312400e-02	4.92531498561398293539370127249816e-05
34	8.64966499042977177325090332415729e-03	3.73103914016284265439688122490895e-05
35	7.30224274879133050003140619052446e-03	2.82375225733516039477667066021446e-05
36	6.16152705009717845830463720403643e-03	2.13513661747602139469739101816769e-05
37	5.19629108350495067218636168760723e-03	1.61297466879220448079982238240246e-05
38	4.37995272297094390520221610919454e-03	1.21739653477311336991048098474804e-05
39	3.68989465744363535075551189083628e-03	9.17991094830884893227377698101798e-06
40	3.10688231013106004394611827804953e-03	6.91584935818872179036239759592572e-06
41	2.61456578557885722141496603598660e-03	5.20536938490202499152488268561648e-06
42	2.19905395393225001547396749458147e-03	3.91430351823738560080383189178292e-06
43	1.84855041619759608964615915855160e-03	2.94070847979427725012698794615673e-06
44	1.55304251639257745230445095694940e-03	2.20719808861136536998364371692094e-06
45	1.30403580024761683344961061119599e-03	1.65508232204597074734186170013816e-06
46	1.09432738764763509113618247317394e-03	1.23989163441506187230543611758337e-06
47	9.17812647645417749658202151298786e-04	9.27962520159008244607471765496508e-07
48	7.69320359699922614599799922262156e-04	6.93835226000040035242065190155287e-07
49	6.44722297506745965386556618727 96e-04	5.18272340903010891482796683060429e-07
50	5.39563219268408452082296554789566e-04	3.86751562364387865498882802928547e-07
51	4.51459652187210048535645581625337e-04	2.88320243535854856966320396641389e-07
52	3.77512500082907183102947952504772e-04	2.14725698524118689197774299181126e-07
53	3.15483620098192985576130479232556e-04	1.59755495420848083506690922212921e-07
54	2.63483041310020855659728424130368e-04	1.18737501808356300532888071897965e-07
55	2.19915670752623096428691515132722e-04	8.81613507227033650558982811933814e-08

k	χ_k	γ_k
56	1.834360266172188275925650253058 02e-04	6.539210585131651461182658543532 09e-08
57	1.529098087894036643347815217341 62e-04	4.845387161336039513882477894319 25e-08
58	1.273812904926187073187057889228 66e-04	3.586641589643111614591182368679 07e-08
59	1.060456634304042235459314591571 07e-04	2.652193458308873709915406597428 50e-08
60	8.822559606230973289380472907723 80e-05	1.959218330263603683618168792426 92e-08
61	7.335137355822449174635956721613 40e-05	1.445856033934328452809654607583 72e-08
62	6.094408110200891073594383828499 30e-05	1.065951937570938313901560579347 50e-08
63	5.060137180108477951033440033553 03e-05	7.851055100610633450758313799650 22e-09
64	4.198542848428867572357563471321 90e-05	5.777040945515843206683059537894 02e-09
65	3.481278678871496035986956479613 78e-05	4.246984556567347716135086192084 12e-09
66	2.884573653448265025396707194415 46e-05	3.119362726958466926330316138880 51e-09
67	2.388506070156355510729919881293 80e-05	2.289148960080258772934255836717 07e-09
68	1.976390743773851550715215740224 80e-05	1.678488423360968003023849006917 26e-09
69	1.634262132836027942583569702114 62e-05	1.229733291153510880769080278144 57e-09
70	1.350438639091731565003388154944 53e-05	9.002464943948266877662411038235 72e-10
71	1.115155558621568249397223169517 89e-05	6.585290181377435734644981062588 84e-10
72	9.202560641706401982468887856876 59e-06	4.813367794250642196593487513545 89e-10
73	7.589312136123594629657164061855 46e-06	3.515366229601170806489727538576 93e-10
74	6.255013491652330254164472663514 98e-06	2.565137890119841402445143911808 57e-10
75	5.152324091795804422236073632601 30e-06	1.869904115318430467786707387250 91e-10
76	4.241816497750165229277096785888 96e-06	1.361500270705838775982073734000 05e-10
77	3.490681068129521098346657220376 69e-06	9.898961255365139488208947938705 82e-11
78	2.871638709042819781233811204998 82e-06	7.184054979517635244481509483186 52e-11
79	2.362029272786446141349385928855 35e-06	5.201486658295414627563990796128 47e-11
80	1.943048852854948439094667675335 74e-06	3.754437199490433204910810890154 06e-11
81	1.599113210650173806417534347908 50e-06	2.698867712598198470474623422276 78e-11
82	1.317327152401696714334777963333 42e-06	1.929419139348942505451442441549 76e-11
83	1.087042114696510170232108154986 90e-06	1.369068265734557083058773404150 78e-11
84	8.994871030284059110792404750527 76e-07	9.615432045370634253902531660339 86e-12
85	7.474609447348354946031506056812 52e-07	6.657655147201540234282022008383 44e-12
86	6.250760128031830729497149967782 14e-07	4.517819685891474356816611387986 25e-12
87	5.275451884078404040349724023647 04e-07	2.977908057967353530561580638597 67e-12
88	4.510052795475430695128400452592 75e-07	1.879705105378246147415887116022 32e-12
89	3.923719667276868476524224601371 22e-07	1.108962425496266433856660647870 54e-12
90	3.492242069352263078951726074125 10e-07	5.839016818701678168028938114292 44e-13
91	3.197199133209018938975521599165 08e-07	2.470550528421158897552296499613 40e-13
92	3.025473256791130577328062653068 83e-07	5.990626808250251912843348664672 65e-14

TABLE 4. Data for Padé approximation of the wave with velocity $c = 1.0922851405$, the steepness $H/\lambda = 0.14105777885488320816492860225696$, and $y_0 = -0.28978481161845687297742961 1644$. Parameters of simulations and Padé approximation are $M = 134217728$, $R(y) \simeq 6.14 \times 10^{-27}$, $err_{pade} \simeq 5.43 \times 10^{-27}$, and the smallest Fourier harmonic had value $|\hat{z}_{k_{max}}| \simeq 3.00 \times 10^{-31}$.

REFERENCES

Alpert, Bradley, Greengard, Leslie & Hagstrom, Thomas 2000 Rapid evaluation of nonreflecting boundary kernels for time-domain wave propagation. *SIAM J. Num. Anal.* **37**, 1138–1164.

Amick, C. J., Fraenkel, L. E. & Toland, J. F. 1982 On the stokes conjecture for the wave of extreme form. *Acta Math.* **148**, 193–214.

Aptekarev, A. I., Buslaev, V. I., Martinez-Finkelshtein, A. & Suetin, S.P. 2011 Padé approximants, continued fractions, and orthogonal polynomials. *Russian Math. Surveys* **88**, 1049–1131.

Baker, Gregory R. & Xie, Chao 2011 Singularities in the complex physical plane for deep water waves. *J. Fluid Mech.* **685**, 83–116.

de Montessus de Ballore, R. 1902 Sur les fractions continues algébriques. *Bull. Soc. Math. France* **30**, 28–36.

Buslaev, V. I. 2001 Simple counterexample to the baker-gammel-wills conjecture. *East J. Approx.* **7**, 515–517.

Chen, B & Saffman, PG 1980 Numerical evidence for the existence of new types of gravity-waves of permanent form on deep-water. *Studies in Applied Mathematics* **62** (1), 1–21.

Cowley, Stephen J., Baker, Greg R. & Tanveer, Saleh 1999 On the formation of moore curvature singularities in vortex sheets. *J. Fluid Mech.* **378**, 233–267.

Drennan, W.M., Hui, W.H. & Tenti, G. 1992 Accurate calculations of stokes water waves of large amplitude. *Zeitschrift f ur angewandte Mathematik und Physik ZAMP* **43** (2), 367–384.

Dyachenko, Alexander I., Kuznetsov, Evgenii A., Spector, Michael & Zakharov, Vladimir E. 1996*a* Analytical description of the free surface dynamics of an ideal fluid (canonical formalism and conformal mapping). *Phys. Lett. A* **221**, 73–79.

Dyachenko, A. I., Zakharov, V. E. & Kuznetsov, E. A. 1996*b* Nonlinear dynamics of the free surface of an ideal fluid. *Plasma Physics Reports* **22**, 829–840.

Dyachenko, Sergey A., Lushnikov, Pavel M. & Alexander O. Korotkevich, http://stokeswave.org 2015 .

Dyachenko, Sergey A., Lushnikov, Pavel M. & Korotkevich, Alexander O. 2013 The complex singularity of a stokes wave. *JETP Letters* **98** (11), 767–771.

Frigo, Mateo & Johnson, Steven G. 2005 The design and implementation of fftw 3, http://fftw.org. *Proc. IEEE* **93** (2), 216–231.

G. A. Baker, Jr. & Graves-Morris, P. R. 1996 *Padé Approximants, 2nd ed.,*. Cambridge: Cambridge Univ. Press.

Gakhov, F. D. 1966 *Boundary Value Problems*. New York: Pergamon Press.

Gandzha, I. S. & Lukomsky, V. P. 2007 On water waves with a corner at the crest. *Proc. R. Soc. A* **463**, 1597.

GNU Project, http://gnu.org 1984-2012 .

Gonchar, A. A. 1973 On the convergence of padé approximants. *Math. USSR Sb.* **21**, 155–166.

Gonchar, A. A. 1975 On the convergence of generalized padé approximants of meromorphic functions. *Math. USSR Sb.* **27**, 503–514.

Gonnet, Pedro, Pachon, Ricardo & Trefethen, Lloyd N. 2011 Robust rational interpolation and least-squares. *Electronic Transactions on Numerical Analysis* **1388**, 146–167.

Grant, Malcolm A. 1973 The singularity at the crest of a finite amplitude progressive stokes wave. *J. Fluid Mech.* **59(2)**, 257–262.

Hestenes, Magnus R. & Stiefel, Eduard 1952 Methods of conjugate gradients for solving linear systems. *J. Research of Nat. Bureau of Standards* **49** (6), 409–436.

Inogamov, N. A. & Oparin, A. M. 2003 Bubble motion in inclined pipes. *Journal of Experimental and Theoretical Physics* **97**, 1168–1185.

Kuznetsov, E.A., Spector, M.D. & Zakharov, V.E. 1993 Surface singularities of ideal fluid. *Physics Letters A* **182** (4-6), 387 – 393.

Kuznetsov, E. A., Spector, M. D. & Zakharov, V. E. 1994 Formation of singularities on the free surface of an ideal fluid. *Phys. Rev. E* **49**, 1283–1290.

Lakoba, Taras I. & Yang, J. 2007 A generalized petviashvili iteration method for scalar and

vector hamiltonian equations with arbitrary form of nonlinearity. *J. Comput. Phys.* **226**, 1668–1692.

Lau, S. R. 2004 Rapid evaluation of radiation boundary kernels for time-domain wave propagation on blackholes: implementation and numerical tests. *Class. Quantum Grav* **21**, 4147–4192.

Longuet-Higgins, Michael S. 2008 On an approximation to the limiting stokes wave in deep water. *Wave Motion* **45**, 770–775.

Longuet-Higgins, M. S. & Fox, M. J. H. 1977 Theory of the almost-highest wave: the inner solution. *J. Fluid Mech.* **80(4)**, 721–741.

Longuet-Higgins, M. S. & Fox, M. J. H. 1978 Theory of the almost-highest wave. part 2. matching and analytic extension. *J. Fluid Mech.* **85(4)**, 769–786.

Lubinsky, D. S. 2003 Rogers-ramanujan and the baker-gammel-wills (padé) conjecture. *Ann. of Math.* **157**, 847–889.

Luenberger, David G. 1970 The conjugate residual method for constrained minimization problems. *SIAM J. Numer. Anal.* **7** (3), 390–398.

Lushnikov, P. M. 2001 Dispersion-managed soliton in a strong dispersion map limit. *Opt. Lett.* **26**, 1535 – 1537.

Lushnikov, P. M. 2004 Exactly integrable dynamics of interface between ideal fluid and light viscous fluid. *Physics Letters A* **329**, 49 – 54.

Markoff, A. 1895 Deux démonstrations de la convergence de certaines fractions continues. *Acta Math.* **19**, 93–104.

Meison, D., Orzag, S. & Izraely, M. 1981 Applications of numerical conformal mapping. *J. Comput. Phys.* **40**, 345–360.

Michell, John H. 1893 The highest waves in water. *Phil. Mag. Series 5* **36**, 430–437.

Mineev-Weinstein, Mark, Wiegmann, Paul B & Zabrodin, Anton 2000 Integrable structure of interface dynamics. *Physical Review Letters* **84** (22), 5106–5109.

Moore, D. W. 1979 The spontaneous appearance of a singularity in the shape of an evolving vortex sheet. *Proceedings of the Royal Society of London A: Mathematical, Physical and Engineering Sciences* **365** (1720), 105–119.

Nekrasov, Aleksandr I. 1921 On steady waves. *Izv. Ivanovo-Voznesensk. Polytech. Inst.* **3**, 52–56.

Nekrasov, Aleksandr I. 1951 *The exact theory of standing waves on the surface of heavy fluid*. Moscow: Izdat. Akad. Nauk. SSSR.

Nuttall, J. 1970 The convergence of padé approximants of meromorphic functions. *J. Math. Anal. Appl.* **31**, 147–153.

Ovsyannikov, Lev V. 1973 Dynamics of a fluid. *M.A. Lavrent'ev Institute of Hydrodynamics Sib. Branch USSR Ac. Sci.* **15**, 104–125.

Pelinovsky, D.E. & Stepanyants, Yu.A. 2004 Convergence of petviashvili's iteration method for numerical approximation of stationary solutions of nonlinear wave equations. *SIAM J. Numer. Anal.* **42**, 1110–1127.

Petviashvili, Vladimir I. 1976 Equation for an extraordinary soliton. *Sov. J. Plasma Phys.* **2**, 257–258.

Plotnikov, P.I. 1982 A proof of the stokes conjecture in the theory of surface waves. *Dinamika Splosh. Sredy (In Russian. English translation Stud. Appl. Math.3, 217-244 (2002))* **57**, 41–76.

Polyanin, Andrei D. & Manzhirov, Alexander V. 2008 *Handbook of Integral Equations: Second Edition*. Boca Raton: Chapman and Hall/CRC.

Rainey, R. C. T. & Longuet-Higgins, Michael S. 2006 A close one-term approximation to the highest stokes wave on deep water. *Ocean Engineering* **33**, 2012–2024.

Saff, E. B. 1972 An extension of montessus de ballore's theorem on the convergence of interpolating rational functions. *J. Approximation Theory* **6**, 63–67.

Schwartz, Leonard W. 1974 Computer extension and analytic continuation of stokes' expansion for gravity waves. *J. Fluid Mech.* **62(3)**, 553–578.

Sretenskii, Leonid N. 1976 *Theory of wave motion of fluid*. Moscow: Nauka.

Stahl, H. 1985*a* Extremal domains associated with an analytic function, i. *Complex Variables Theory Appl.* **4**, 311–324.

Stahl, H. 1985*b* Extremal domains associated with an analytic function, ii. *Complex Variables Theory Appl.* **4**, 321–338.

Stahl, H. 1997 The convergence of padé approximants to functions with branch points. *J. Approx. Theory* **91**, 139–204.

Stokes, George G. 1847 On the theory of oscillatory waves. *Transactions of the Cambridge Philosophical Society* **8**, 441–455.

Stokes, George G. 1880*a* On the theory of oscillatory waves. *Mathematical and Physical Papers* **1**, 197–229.

Stokes, George G. 1880*b* Supplement to a paper on the theory of oscillatory waves. *Mathematical and Physical Papers* **1**, 314–326.

Tanveer, S. 1991 Singularities in water waves and rayleigh-taylor instability. *Proc. R. Soc. Lond. A* **435**, 137–158.

Tanveer, S. 1993 Singularities in the classical rayleigh-taylor flow: formation and subsequent motion. *Proc. R. Soc. Lond. A* **441**, 501–525.

Toland, J. F. 1978 On the existence of a wave of greatest height and stokes's conjecture. *Proc. R. Soc. Lond. A* **363**, 469–485.

Turitsyn, S. K., Lai, L., & Zhang, W. W. 2009 Asymmetric disconnection of an underwater air bubble: Persistent neck vibrations evolve into a smooth contact. *Phys. Rev. Lett.* **103**, 124501.

Williams, J. M. 1981 Limiting gravity waves in water of finite depth. *Phil. Trans. R. Soc. Lond. A* **302(1466)**, 139–188.

Williams, John M 1985 *Tables of Progressive Gravity Waves*. London: Pitman.

Wu, S. 2009 Almost global wellposedness of the 2-d full water wave problem. *Invent. Math* **177**, 45–135.

Wu, S. 2011 Global wellposedness of the 3-d full water wave problem. *Invent. Math* **184**, 125–220.

Yang, Jianke 2009 Newton-conjugate-gradient methods for solitary wave computations. *J Comput. Phys.* **228(18)**, 7007–7024.

Yang, Jianke 2010 *Nonlinear Waves in Integrable and Nonintegrable Systems*. SIAM.

Zakharov, Vladimir E. 1968 Stability of periodic waves of finite amplitude on a surface. *J. Appl. Mech. Tech. Phys.* **9** (2), 190–194.

Zakharov, V. E., Dyachenko, A. I. & Prokofiev, A. O. 2006 Freak waves as nonlinear stage of stokes wave modulation instability. *European Journal of Mechanics B/Fluids* **25**, 677–692.

Zakharov, Vladimir E., Dyachenko, Alexander I. & Vasiliev, Oleg A. 2002*a* New method for numerical simulation of a nonstationary potential flow of incompressible fluid with a free surface. *Eur. J. Mech. B/Fluids* **21**, 283–291.

Zakharov, Vladimir E., Dyachenko, Alexander I. & Vasiliev, Oleg A. 2002*b* New method for numerical simulation of nonstationary potential flow of incompressible fluid with a free surface. *European Journal of Mechanics B/Fluids* **21**, 283–291.

Zakharov, Vladimir E., Korotkevich, Alexander O. & Prokofiev, Alexander O. 2009 On dissipation function of ocean waves due to whitecapping. *AIP Proceedings, CP1168* **2**, 1229–1231.

Zakharov, Vladimir E., Korotkevich, Alexander O., Pushkarev, Andrei & Resio, Donald 2007 Coexistence of weak and strong wave turbulence in a swell propagation. *Phys. Rev. Lett.* **99** (16), 164501.